

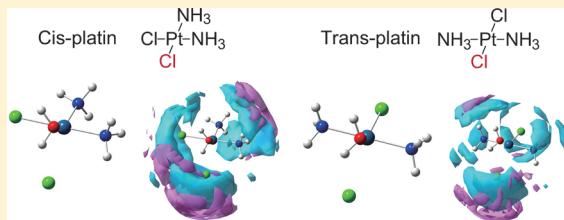
Evaluation Procedure of Electrostatic Potential in 3D-RISM-SCF Method and Its Application to Hydrolyses of Cis- and Transplatin Complexes

Shinji Aono and Shigeyoshi Sakaki*

Fukui Institute for Fundamental Chemistry, Kyoto University, Nishiraki-cho, Takano, Sakyao-ku, Kyoto 606-8103, Japan

Supporting Information

ABSTRACT: In the three-dimensional reference interaction site model self-consistent field (3D-RISM-SCF) method, a switching function was introduced to evaluate the electrostatic potential (ESP) around the solute to smoothly connect the ESP directly calculated with the solute electronic wave function and that approximately calculated with solute point charges. Hydrolyses of cis- and transplatin, *cis*- and *trans*- $\text{PtCl}_2(\text{NH}_3)_2$, were investigated with this method. Solute geometries were optimized at the DFT level with the M06-2X functional, and free energy changes were calculated at the CCSD(T) level. In the first hydrolysis, the calculated activation free energy is 20.8 kcal/mol for cisplatin and 20.3 kcal/mol for transplatin, which agrees with the experimental and recently reported theoretical results. A Cl anion, which is formed by the first hydrolysis, somehow favorably exists in the first solvation shell as a counteranion. The second hydrolysis occurs with a similar activation free energy (20.9 kcal/mol) for cisplatin but a somewhat larger energy (23.2 kcal/mol) for transplatin to afford *cis*- and *trans*-diaqua complexes. The Cl counteranion in the first solvation shell little influences the activation free energy but somewhat decreases the endothermicity in both cis- and transplatin. The present 3D-RISM-SCF method clearly displays the microscopic solvation structure and its changes in the hydrolysis, which are discussed in detail.



1. INTRODUCTION

Solvation effects are crucial in many cases, in particular, polar compounds such as transition metal complexes. This means that the electronic structure calculation incorporating the solvation effect is indispensable. One good example is the polarizable continuum model (PCM), which has been applied to many solution systems.^{1–3} Another is the reference interaction site model self-consistent field (RISM-SCF) method.^{4–7} In this method, a solute molecule is treated by quantum mechanics and surrounding solvents are represented at the level of classical statistical mechanics based on the infinite dilution approximation of one isolated solute. To this aim, the statistical mechanics of a liquid^{4,5} is combined with ab initio molecular orbital theory.^{6,7} As a result, both the solute electronic structure and solvent distribution can be simultaneously evaluated in a self-consistent manner like the PCM. An important difference from the PCM method is that not only the solvation free energy but also the microscopic solvation structure is provided by the RISM-SCF method. In our experience, however, the usual RISM-SCF method, which is called 1D-RISM-SCF (one-dimensional RISM-SCF) hereafter, tends to fail to evaluate the solvation free energy of a bulky and highly polar system owing to two serious problems: one is overestimation of the cavity formation effect, which is inherent in bulky solute molecules such as glucosides and transition metal complexes. The other is the accuracy of the electrostatic potential (ESP), which is approximately evaluated around a solute by effective point charges. These weak points sometimes

suppress wide application of the RISM-SCF method. For instance, we failed to apply 1D-RISM-SCF to the glucoside degradation reaction, because solute partial charges induced divergence in the RISM-SCF cycles,⁸ probably due to its large molecular size and highly polar electronic structure.

The 1D-RISM-SCF-SEDD (spatial electron density distribution) method recently solved the latter problem.⁹ Another powerful method to solve these two problems is the three-dimensional (3D) RISM-SCF method.¹⁰ In the 3D-RISM method, solvent distribution around a solute is represented as a probability density function at 3D grid points, and hence its equilibrium spatial distribution can be obtained from the integral equation theory. In this 3D representation, we can determine the surrounding solvation structure by directly calculating the ESP with the solute electronic wave function, taking into account the solvent spatial configuration. This means that the 3D-RISM method does not need the point charge fitting protocol for solute molecules which sometimes causes unphysical diverged ESP charges of the solute in the RISM-SCF cycles. However, the 3D-RISM-SCF calculation is considerably time-consuming to evaluate the explicit ESP at numerous solvent grid points.

To reduce the computational cost, Yoshida and Hirata proposed to separate 3D space into two regions.¹¹ In one

Received: August 8, 2012

Revised: September 25, 2012

Published: September 26, 2012

region close to a solute, the wave function of the solute was employed to evaluate ESP, but in the other region distant from the solute, the usual point charge fitting protocol was employed.¹² This method does not induce any problem practically, when the inner region is enough widely taken and/or the solute is neither bulky nor highly polarizable. However, this problem would become serious when the solute is bulky and highly polarizable like a transition metal complex. In such a case, the continuity of the ESP at the boundary between these two regions must be considered, which was not considered in the original method.^{11–13} To solve this connection problem, we introduced here a switching region into the solvent grid space. In other words, the 3D space is divided into three regions, i.e., inner, outer, and switching regions; see Figure 1. In the inner region near the solute, the

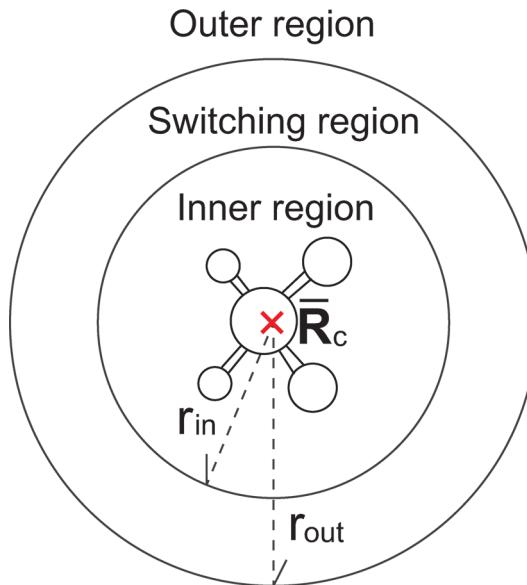
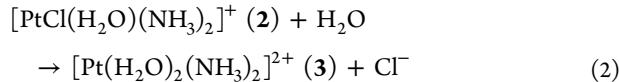
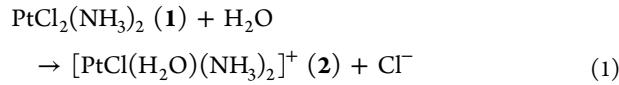


Figure 1. Schematic view of three divided regions around the solute, i.e., inner, outer, and switching regions. \bar{R}_c is the center of the solute.

ESP is directly calculated from the solute electronic wave function. In the outer region distant from the solute, the ESP is approximately estimated by the solute effective charges like the previous method.¹¹ In the switching region between the inner and the outer ones, we newly introduced a switching function to smoothly connect the inner and outer regions. By the use of the switching function, the discontinuity of the solvent distribution was solved for the whole grid space.

In the present work, we constructed the 3D-RISM-SCF method at the density functional theory (DFT) and MP2 levels by employing the switching function to smoothly connect the ESP directly calculated by the wave function and that calculated by the point charge approximation. We also implemented the analytical gradient calculation method at the DFT level under this scheme. We applied this method to the first and second hydrolyses of *cis*-diamminedichloroplatinum(II) (i.e., cisplatin) and its trans isomer (i.e., transplatin). Cisplatin is well-known as an antitumor drug and attracts much attention in both the experimental and theoretical fields.^{14,15} Interestingly, cisplatin exhibits anticancer activity, while transplatin does not. From the experimental X-ray analysis, the difference between *cis*- and transplatin has been discussed in terms of the cross-link adduct formation between the complex and two guanine DNA bases of

cancer cells in the human body.¹⁶ Prior to this cross-link reaction, it is generally believed that the hydrolysis of the complex occurs as the first step:



where eqs 1 and 2 are the first and second hydrolyses, respectively. For simplicity, we hereafter name *cis*- $\text{PtCl}_2(\text{NH}_3)_2$, *cis*- $[\text{PtCl}(\text{H}_2\text{O})(\text{NH}_3)_2]^+$, and *cis*- $[\text{Pt}(\text{H}_2\text{O})_2(\text{NH}_3)_2]^{2+}$ as $\mathbf{1}_{\text{cis}}$, $\mathbf{2}_{\text{cis}}$, and $\mathbf{3}_{\text{cis}}$, respectively, and the corresponding trans isomers as $\mathbf{1}_{\text{tr}}$, $\mathbf{2}_{\text{tr}}$, and $\mathbf{3}_{\text{tr}}$. The second hydrolysis in eq 2 is also considered to occur before the cross-link reaction, but the reaction rate is experimentally reported to be slow.^{17,18} Actually, the NMR experiments indicate that the monoqua complex $\mathbf{2}_{\text{cis}}$ is found but the diaqua complex $\mathbf{3}_{\text{cis}}$ is not.^{19,20}

To investigate these hydrolyses and DNA-binding reactions, various computational studies have been carried out. In those studies, the PCM method was used to incorporate the solvation effect.^{21–28} It is well-known that the PCM method does not capture local structures of hydrogen bonds between a solute complex and water solvents. Also, microscopic solvation structure is not presented by this method. To clarify the microscopic solvation structure, Monte Carlo simulation was employed.²⁹ In this study, however, bond breaking and formation in the hydrolysis could not be discussed owing to the limitation of the classical mechanics. Car–Parrinello molecular dynamics (CPMD) simulations were carried out for cisplatin.^{30–32} Though this method is based on a more reliable model of solute–solvent interaction, there are still several problems; for example, the number of water solvent molecules is not enough to represent solvation effects in a charged system, as pointed out by Lopes et al.²⁹ Also, the dissociation process cannot be sufficiently investigated owing to the limitation of solvent box size. As an alternative study, the 1D-RISM-SCF-SEDD method was recently applied to the hydrolysis of cisplatin by Yokogawa et al. and the importance of solvation in this hydrolysis was well discussed.³³

Considering the strong points of the 3D-RISM-SCF method discussed above, we believe that the solvation of transition metal complexes must be investigated with the 3D-RISM-SCF method after improving the ESP evaluation method; see below for details of the improvement. Here, we selected the hydrolysis of cisplatin reaction for the first application of this 3D-RISM-SCF method, because this hydrolysis has been well investigated so far. Also, we wish to explore the hydrolysis of transplatin, to make a comparison between *cis*- and transplatin, and to investigate *cis*–*trans* isomerizations of platin and hydrolysis product, because these issues are of considerable importance in the chemistry of cisplatin but have not been investigated well. In particular, the *cis*–*trans* isomerization has not been theoretically studied at all, despite the experimental observation of *cis*–*trans* isomerization in aqueous solution.^{34,35} In this work, we wish to present a comprehensive theoretical study of the chemistry of *cis*- and transplatin.

In section 2, we describe how the ESP is evaluated with the switching region and the energy and gradient calculations in the present 3D-RISM-SCF method. In section 3, we mention computational details to investigate the hydrolysis reactions of

cis- and transplatin. In section 4, we discuss solvation free energies and solvation structures evaluated by the 3D-RISM-SCF method. To clarify the essence of the solvation effect on the hydrolysis processes of these two isomers, we performed the free energy decomposition analysis of solvation by employing the linear response theory, which provides the solvation free energy as half of the average solute–solvent interaction energy. Our conclusions are summarized in section 5.

2. THEORETICAL METHOD

2.1. 3D-RISM Integral Equation. We wish to present here a minimum description of the RISM theory, because it is necessary to present a new computational scheme of the ESP. For solvent spatial distribution in equilibrium with solute electronic and nuclear structures, the solute–solvent 3D-RISM equation is given as follows:

$$c_\xi(\mathbf{r}) = \begin{cases} \exp[-\beta u_\xi(\mathbf{r}) + \eta_\xi(\mathbf{r})] - \eta_\xi(\mathbf{r}) - 1 & \text{for } -\beta u_\xi(\mathbf{r}) + \eta_\xi(\mathbf{r}) < 0 \\ -\beta u_\xi(\mathbf{r}) & \text{for } -\beta u_\xi(\mathbf{r}) + \eta_\xi(\mathbf{r}) \geq 0 \end{cases} \quad (5)$$

where u_ξ is the interaction potential between the solute molecule and solvent site ξ . β is $1/k_B T$, where k_B and T are the Boltzmann constant and temperature, respectively. To evaluate the free energy, we used the hypernetted chain (HNC) closure, eq 6, because this HNC closure is believed to provide the better free energy.

$$c_\xi(\mathbf{r}) = \exp[-\beta u_\xi(\mathbf{r}) + \eta_\xi(\mathbf{r})] - \eta_\xi(\mathbf{r}) - 1 \quad (6)$$

Iteratively solving eqs 4 and 5 (or eqs 4 and 6), we can obtain the correlation functions, c_ξ and η_ξ . According to eq 3, these correlation functions give the solvent spatial distribution function g_ξ , where g_ξ is equal to $h_\xi + 1$. However, this iteration cycle involves the forward and backward 3D fast Fourier transformation (FFT). Thus, we have to pay attention to the treatment of the long-range Coulomb potential in c_ξ ; see Supporting Information, pages S2 and S3, for a summary of the present procedure to solve the integral equation.

2.2. Divided Regions for ESP Calculation. The interaction potential in eq 5 is defined as the sum of electrostatic (ES) and Lennard-Jones (LJ) potentials between the solute molecule and the solvent site, according to the proposal by Yoshida and Hirata.

$$u_\xi(\mathbf{r}) = u_\xi^{\text{ES}(e)}(\mathbf{r}) + u_\xi^{\text{ES}(n)}(\mathbf{r}) + u_\xi^{\text{LJ}}(\mathbf{r}) \quad (7)$$

where $u^{\text{ES}(e)}$ and $u^{\text{ES}(n)}$ are the ESPs provided by the solute electrons and nuclei, respectively. The LJ potential, u_ξ^{LJ} , is represented by the site–site representation

$$u_\xi^{\text{LJ}}(\mathbf{r}) = \sum_b 4\epsilon_{b\xi} \left\{ \left(\frac{\sigma_{b\xi}}{|\mathbf{r} - \mathbf{R}_b|} \right)^{12} - \left(\frac{\sigma_{b\xi}}{|\mathbf{r} - \mathbf{R}_b|} \right)^6 \right\} \quad (8)$$

where \mathbf{R}_b is the Cartesian coordinate of solute site b . The electrostatic potentials, $u^{\text{ES}(e)}$ and $u^{\text{ES}(n)}$, can be represented with the density matrix, $D_{\mu\nu}$, as follows:

$$u_\xi^{\text{ES}(e)}(\mathbf{r}) = -q_\xi^V \sum_{\mu\nu} D_{\mu\nu} A_{\mu\nu}(\mathbf{r}) \quad (9)$$

$$\tilde{\eta}_\xi(\mathbf{k}) = \tilde{h}_\xi(\mathbf{k}) - \tilde{c}_\xi(\mathbf{k}) \quad (3)$$

$$\tilde{\eta}_\xi(\mathbf{k}) = \sum_\gamma \tilde{c}_\gamma(\mathbf{k}) [\tilde{\omega}_{\gamma\xi}^V(k) + \rho^V \tilde{h}_{\gamma\xi}^{VV}(k)] - \tilde{c}_\xi(\mathbf{k}) \quad (4)$$

where ρ^V is the number density of solvent molecules, the tilde denotes the quantity in reciprocal space, c_ξ and h_ξ are the direct and the total correlation functions for solvent site ξ , respectively, ω^V is the solvent intramolecular correlation function, and h^{VV} is the solvent–solvent total correlation function obtained by solving the solvent–solvent 1D-RISM equation. To solve the solute–solvent total correlation function, h_ξ , one more other closure relation is required. In the present calculations, we used the Kovalenko–Hirata (KH) closure, eq 5, for geometry optimization.

$$u_\xi^{\text{ES}(n)}(\mathbf{r}) = q_\xi^V \sum_b \frac{Z_b}{|\mathbf{r} - \mathbf{R}_b|} \quad (10)$$

where q_ξ^V is the point charge of solvent site ξ , Z_b is the nuclear charge of solute site b , and $A_{\mu\nu}$ is the one-electron integral represented by atomic basis functions χ_μ and χ_ν ; see eq 11.

$$A_{\mu\nu}(\mathbf{r}) = \int d\mathbf{r}' \chi_\mu^*(\mathbf{r}') \frac{1}{|\mathbf{r} - \mathbf{r}'|} \chi_\nu(\mathbf{r}') \quad (11)$$

Compared with the calculations of $u_\xi^{\text{ES}(n)}$ and u_ξ^{LJ} in the entire space, the estimation of $u_\xi^{\text{ES}(e)}$ in eq 9 needs a considerably long computational time. To reduce the computational time, we divided the solvent grid space into three regions, i.e., inner, outer, and switching regions, as shown in Figure 1. For simplicity, we separated these regions by the spherical area depending on the distance between the center of the solute molecule and the solvent grid point. One of the merits in this spherical division is that the rotational invariance can be satisfied automatically. The inner region near the solute is defined so as to cover the first and second solvation shells at least. In this region, we estimated the ESP with eq 9, because the accurate description of ESP is necessary to the correct evaluation of the solvation structure. The outer region is defined so as to be sufficiently distant from the solute, in which the ESP can be approximately evaluated as the sum of Coulomb potentials provided by the solute electronic point charges, \mathbf{Q} . The solute electronic point charges can be presented in the same manner as the 1D-RISM method, where the electronic point charge matrix $Q_{\mu\nu}^b$ is obtained by the least-squares fitting protocol.⁶

$$Q_b = \sum_{\mu\nu} D_{\mu\nu} Q_{\mu\nu}^b \quad (12)$$

The switching region is defined between the inner and the outer ones. In this region, we evaluated the ESP by two different protocols. One is the direct calculation of eq 9, and the other is the approximate estimation with the solute electronic point charges. To smoothly connect these two ESPs, we employ a switching function to satisfy the condition that it is

monotonically damped from 1 to 0 and also its first derivative becomes zero at both of the boundaries to the inner and outer regions.

Thus, the ESPs in the three regions can be represented by eq 13.

$$u_{\xi}^{\text{ES}(e)}(\mathbf{r}) = -q_{\xi}^V \left\{ w_i(\mathbf{r}) \sum_{\mu\nu} D_{\mu\nu} A_{\mu\nu}(\mathbf{r}) - w_o(\mathbf{r}) \sum_b \frac{Q_b}{|\mathbf{r} - \mathbf{R}_b|} \right\} \quad (13)$$

where

$$w_i(\mathbf{r}) \equiv \begin{cases} 1 & \text{for } |\mathbf{r} - \bar{\mathbf{R}}_c| \leq r_{\text{in}} \\ 0 & \text{for } |\mathbf{r} - \bar{\mathbf{R}}_c| \geq r_{\text{out}} \\ \text{Sw}(|\mathbf{r} - \bar{\mathbf{R}}_c|) & \text{otherwise} \end{cases}$$

and $w_o(\mathbf{r}) \equiv 1 - w_i(\mathbf{r})$

Here, $\bar{\mathbf{R}}_c$ is the center of the solute molecule and Sw is the switching function to smoothly connect the ESPs between the inner and outer regions. In the present calculations, the switching function, $\text{Sw}(x)$, is defined by eq 15:

$$\text{Sw}(x') = 1 - x'^3 \{10 - x'(15 - 6x')\}$$

for $0 \leq x' \equiv \frac{x - r_{\text{in}}}{r_{\text{out}} - r_{\text{in}}} \leq 1$

2.3. Solvated Fock Matrix. To take into account the electronic polarization of solute induced by solvent molecules, we construct the solvated Fock matrix by dividing the solvent space into the inner, outer, and switching regions. This is extended from the original 3D-RISM-SCF method,¹¹ as follows: Adding the one-electron operator term of the solute–solvent interaction to the Fock matrix in the gas phase, $\mathcal{F}_{\mu\nu}^{\text{gas}}$, the solvated Fock matrix, $\mathcal{F}_{\mu\nu}^{\text{solv}}$, can be represented by eq 16.

$$\mathcal{F}_{\mu\nu}^{\text{solv}} = \mathcal{F}_{\mu\nu}^{\text{gas}} - \rho^V \sum_{\xi} q_{\xi}^V \int_{\text{all}} d\mathbf{r} \left\{ w_i(\mathbf{r}) A_{\mu\nu}(\mathbf{r}) g_{\xi}(\mathbf{r}) - w_o(\mathbf{r}) \sum_b \frac{Q_{\mu\nu}^b}{|\mathbf{r} - \mathbf{R}_b|} g_{\xi}(\mathbf{r}) \right\} \quad (16)$$

where $w_i(\mathbf{r})$ and $w_o(\mathbf{r})$ denote the same weight functions as in eq 14, respectively. To calculate $A_{\mu\nu}(\mathbf{r})$, the conventional transformation was used, as follows:

$$A_{\mu\nu}(\mathbf{r}) = \frac{2}{\pi} \int d\mathbf{r}' \int_0^{\infty} du \exp[-u^2 |\mathbf{r}' - \mathbf{r}|^2] \chi_{\mu}^{*}(\mathbf{r}') \chi_{\nu}(\mathbf{r}') \quad (17)$$

To simply evaluate the integration on the right-hand side of eq 17, we take the integral of a three-center Gaussian with respect to \mathbf{r}' by the Gauss–Hermite quadrature and then we take this integral with respect to u by the Rys quadrature.³⁶ Because the computational costs mainly depend on this integration of $A_{\mu\nu}(\mathbf{r})$ in eqs 13 and 16,³⁷ the division of solvent grid space is powerful enough to reduce the computational time.

2.4. Free Energy Gradient Calculation. Solving the solvated Fock matrix, $\mathcal{F}_{\mu\nu}^{\text{solv}}$, in eq 16, we can obtain the solute electronic wave function, Φ_{solv} , in equilibrium with the solvent spatial distribution, $\{g_{\xi}(\mathbf{r})\}$. The total free energy of the solute–solvent system, F , is defined as the sum of the solute electronic energy, E_{solute} , and the excess chemical potential, $\Delta\mu$, (i.e., solvation free energy).

$$F = E_{\text{solute}} + \Delta\mu \quad (18)$$

$$E_{\text{solute}} = \langle \Phi_{\text{solv}} | \hat{H}_{\text{gas}} | \Phi_{\text{solv}} \rangle \quad (19)$$

where \hat{H}_{gas} is the gas phase electronic Hamiltonian. If we use the KH closure, the excess chemical potential, $\Delta\mu$, is given by eq 20.

$$\Delta\mu = \frac{\rho^V}{\beta} \sum_{\xi} \int d\mathbf{r} \left[\frac{1}{2} h_{\xi}^2(\mathbf{r}) \Theta(-h_{\xi}(\mathbf{r})) - c_{\xi}(\mathbf{r}) - h_{\xi}(\mathbf{r}) c_{\xi}(\mathbf{r}) \right] \quad (20)$$

where Θ is the Heaviside step function. The correlation functions in eq 20 are evaluated with the 3D-RISM-SCF method. Note that, in the case of HNC closure, the first term in eq 20 disappears in the definition of excess chemical potential.

Because the present 3D-RISM-SCF method is based on the variational principle, we do not need to evaluate the derivative of the linear combination of atomic orbitals (LCAO) coefficient in the same manner as the usual gradient calculation in gas phase. As a result, the analytical energy gradient of F is represented by

$$\begin{aligned} \frac{\partial F}{\partial \mathbf{R}_a} = & -\rho^V \sum_{\mu\nu} D_{\mu\nu} \sum_{\xi} \left[q_{\xi}^V \int_{\text{all}} d\mathbf{r} \right. \\ & g_{\xi}(\mathbf{r}) \frac{\partial}{\partial \mathbf{R}_a} \left\{ w_i(\mathbf{r}) A_{\mu\nu}(\mathbf{r}) - w_o(\mathbf{r}) \sum_b \frac{Q_{\mu\nu}^b}{|\mathbf{r} - \mathbf{R}_b|} \right\} \\ & + \rho^V \sum_{\xi} \left[\int_{\text{all}} d\mathbf{r} g_{\xi}(\mathbf{r}) \frac{\partial u_{\xi}^{\text{LJ}}}{\partial \mathbf{R}_a} \right. \\ & \left. \left. + q_{\xi}^V \int_{\text{all}} d\mathbf{r} g_{\xi}(\mathbf{r}) \frac{\partial}{\partial \mathbf{R}_a} \sum_b \frac{Z_b}{|\mathbf{r} - \mathbf{R}_b|} \right] \right] \end{aligned} \quad (21)$$

Note that the derivatives of weight functions, $\partial w_i / \partial \mathbf{R}_a$ and $\partial w_o / \partial \mathbf{R}_a$, must be calculated in eq 21, because they are dependent on the molecular center, $\bar{\mathbf{R}}_c$. The derivatives of electronic point charges, $\partial Q_{\mu\nu}^b / \partial \mathbf{R}_a$, are evaluated with the same method employed in the 1D-RISM calculation.⁷ Thus, the energy gradient calculation based on the variational principle can be carried out without difficulty.

2.5. Correction of Basis Set Superposition Error (BSSE)

in RISM-MP2 Calculation. In the RISM-MP2 method, we can make the BSSE correction by following the counterpoise method.³⁸ From the analogy with the 1D-RISM-RHF/MP2 method with the pure point charge approximation,³⁹ the second order correlation free energy at the MP2 level, $F^{(2)}$, is defined in the present 3D-RISM-RHF/MP2 method, as follows:

$$F^{(2)} = E_{\text{solute}}^{(2)} + \Delta\mu^{(2)} \quad (22)$$

where the second order electronic energy of the solute, $E_{\text{solute}}^{(2)}$, can be represented by modifying the conventional form of the gas phase correlation energy, as follows:

$$\begin{aligned} E_{\text{solute}}^{(2)} = & \frac{1}{4} \sum_{ij,ab} \frac{|\langle ij||ab \rangle|^2}{\epsilon_i + \epsilon_j - \epsilon_a - \epsilon_b} \\ & + \rho^V \sum_{\mu\nu} D_{\mu\nu}^{(2)} \sum_{\xi} q_{\xi}^V \int_{\text{all}} d\mathbf{r} \left\{ w_i(\mathbf{r}) A_{\mu\nu}(\mathbf{r}) \right. \\ & \left. - w_o(\mathbf{r}) \sum_b \frac{Q_{\mu\nu}^b}{|\mathbf{r} - \mathbf{R}_b|} \right\} g_{\xi}(\mathbf{r}) \end{aligned} \quad (23)$$

where i and j represent the occupied molecular orbitals (MOs), a and b represent the unoccupied MOs, ϵ_x is the orbital energy of the x th MO, and $D_{\mu\nu}^{(2)}$ is the second order density matrix. When the solvent distribution function is in equilibrium with the electronic structure of the solute, $\Delta\mu^{(2)}$ in eq 22 can be also obtained by eq 24.

$$\begin{aligned} \Delta\mu^{(2)} = & -\rho^V \sum_{\mu\nu} D_{\mu\nu}^{(2)} \sum_{\xi} q_{\xi}^V \int_{\text{all}} d\mathbf{r} \\ & \left\{ w_i(\mathbf{r}) A_{\mu\nu}(\mathbf{r}) - w_o(\mathbf{r}) \sum_b \frac{Q_{\mu\nu}^b}{|\mathbf{r} - \mathbf{R}_b|} \right\} g_{\xi}(\mathbf{r}) \end{aligned} \quad (24)$$

As a result of eqs 23 and 24, $F^{(2)}$ can be provided in the simple form

$$F^{(2)} = \frac{1}{4} \sum_{ij,ab} \frac{|\langle ij||ab \rangle|^2}{\epsilon_i + \epsilon_j - \epsilon_a - \epsilon_b} \quad (25)$$

To make the BSSE correction of free energy for a supermolecule, $\Delta F_{\text{BSSE}}^{(2)}$, we need to evaluate the difference between the second order electronic energy of monomer, $E_{\text{mono}(i)}^{(2)}$, calculated with ghost basis sets and that calculated without ghost basis sets. As an important point, these energy calculations of the monomers must be carried out under the solvent configuration in equilibrium with the solute charge distribution of the supermolecule. To this aim, we initially calculate the supermolecular system to obtain the surrounding solvent distribution, $\{g_{\xi}^{\text{sup}}(\mathbf{r})\}$. Then, freezing the obtained solvent distribution, $\{g_{\xi}^{\text{sup}}(\mathbf{r})\}$, we evaluate the electronic energy corrections for all the monomers, $\Delta_G E_{\text{mono}(i)}^{(2)}$; Δ_G represents the following operation on the quantity, X .

$$\Delta_G X \equiv X_{-} - X_{+} \quad (26)$$

where X_{-} and X_{+} are the expectation values calculated with and without ghost basis sets, respectively. Applying the counterpoise method to the estimation of $\Delta\mu^{(2)}$ in eq 24 with the fixed solvent distribution, $\{g_{\xi}^{\text{sup}}(\mathbf{r})\}$, we also approximately estimate the BSSE correction of solvation free energy for each monomer, $\Delta_G \Delta\mu_{\text{mono}(i)}^{(2)}$. As a result of the summation of the $\Delta_G E_{\text{mono}(i)}^{(2)}$ and $\Delta_G \Delta\mu_{\text{mono}(i)}^{(2)}$ terms on all the monomers $\{i\}$, we can obtain the BSSE correction for the supermolecular system, as follows:

$$\Delta F_{\text{BSSE}}^{(2)} = \sum_i^{\text{monomer}} \{\Delta_G E_{\text{mono}(i)}^{(2)} + \Delta_G \Delta\mu_{\text{mono}(i)}^{(2)}\} \quad (27)$$

The above BSSE correction in the RISM-SCF method is similar to that in the PCM method,⁴⁰ as follows: In the PCM method, we also initially define the cavity surface, which

determines the apparent surface charges in the supermolecular system, and then we calculate all the free energy corrections for monomers by freezing the obtained cavity surface about the supermolecular system.

3. COMPUTATIONAL DETAILS

The geometry optimization was carried out by the DFT method with the M06-2X functional, as will be explained in section 4. To solve the 3D-RISM integral equation, we employed the KH closure. The LANL08(f) basis sets were used for valence electrons of Pt, where its 60 core electrons were replaced with the Hay–Wadt effective core potential (ECP). For all the remaining atoms, the 6-31++G** basis sets were used. This basis set system is hereafter named BS-I. The free energy profile was calculated by the MP2 perturbation theory with better basis sets; while the same basis set and ECP as those of BS-I were employed for Pt, the cc-pVTZ basis sets were used for the other atoms, where diffuse functions were added to Cl and O. This basis set system is hereafter named BS-II. In the calculation of free energy at the MP2 level, the MP2 correlation energy was added after solving the 3D-RISM-SCF cycle at the RHF level with the HNC closure (hereafter named 3D-RISM-RHF/MP2). To accurately evaluate the correlation energy, we also performed the CCSD(T) calculation by replacing the aug-cc-pVTZ and cc-pVTZ basis sets in the BS-II with the aug-cc-pVDZ and cc-pVDZ basis sets, respectively. This basis set system is hereafter named BS-III. In the calculation of free energy at the CCSD(T) level, we evaluated the difference in correlation energy between 3D-RISM-RHF/MP2 and 3D-RISM-RHF/CCSD(T) with the BS-III and then added it to the corresponding MP2 free energy obtained by 3D-RISM-RHF/MP2 with the BS-II; this computational scheme corresponds to the free energy calculation at the CCSD(T) level with the BS-II, where the basis set extension effect from the BS-III to the BS-II is approximately evaluated at the MP2 level. The BSSE correction was included at the level of the 3D-RISM-RHF/MP2 computation with the BS-II. The zero point energy, thermal energy, and entropy of the solute molecule were evaluated, as follows: The vibrational frequencies calculated by the PCM method with the BS-I were employed for evaluation of the vibrational entropy and thermal energy. The translational entropy in the condensed phase was calculated with the modified free volume, as proposed by Mammen et al.⁴¹

As the initial step of the 3D-RISM-SCF method, the 1D-RISM calculation was carried out to set up the solvent–solvent total correlation functions at the density $\rho^V = 0.997 \text{ g/cm}^3$ and temperature $T = 298.15 \text{ K}$. The point charges and LJ parameters of water solvents were taken from the simple point charge (SPC) model⁴² by modifying the LJ parameters of the H atom: $\sigma_{\text{Hw}} = 1.0 \text{ \AA}$ and $\epsilon_{\text{Hw}} = 0.056 \text{ kcal/mol}$.^{6,7} For convenience, “Hw” represents the H site of H_2O and “Ha” represents the H site of NH_3 hereafter. The 1D-RISM calculation was performed on a grid of 1024 points, corresponding to the 1D space radius of 56.2 Å. In the 3D-RISM calculation, the LJ parameters of solute molecules were taken from AMBER⁴³ except for Pt. For Pt, we determined the LJ parameters by fitting the MP2 potential energy profile of cis- and transplatin complexes with one water molecule: $\sigma_{\text{Pt}} = 4.75 \text{ \AA}$ and $\epsilon_{\text{Pt}} = 0.070 \text{ kcal/mol}$. These LJ parameters of Pt are very close to those of the previous work by Hayaki et al.⁴⁴ As a box size of solvents, we set a cubic grid of 128 points/axis with the spacing of 0.5 Å for the free energy calculation and the

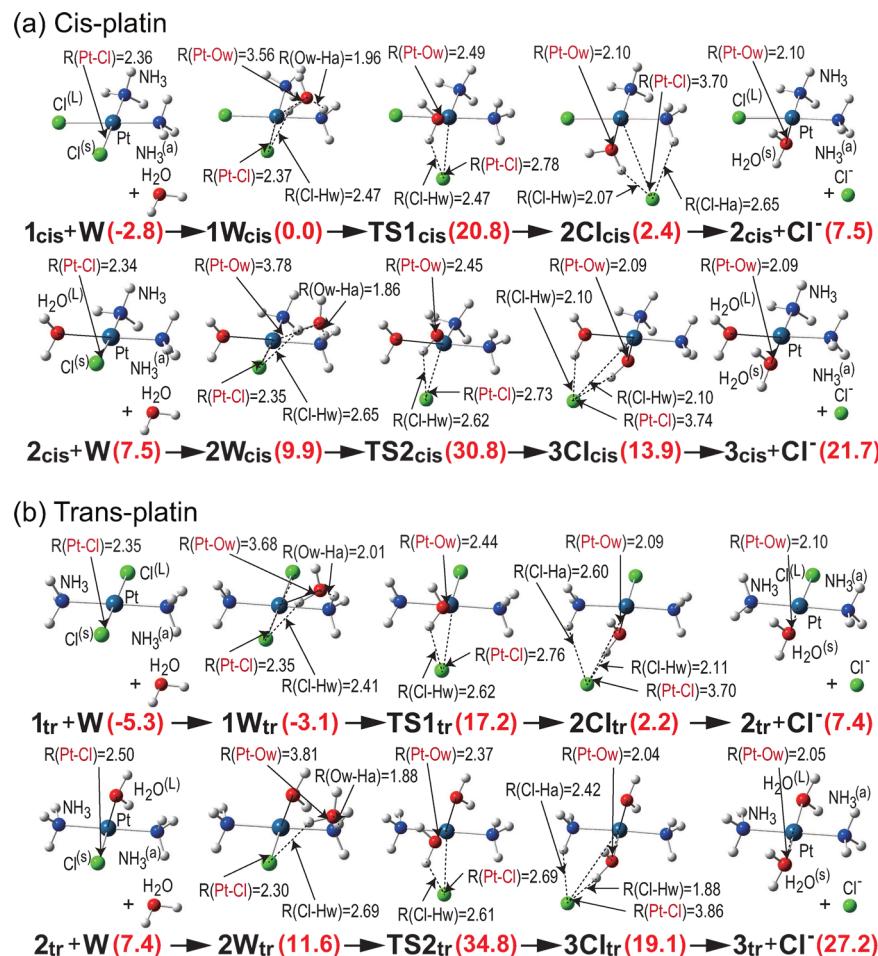


Figure 2. Geometry and CCSD(T)-calculated free energy changes in the first and second hydrolyses of cis- and transplatin. (a) Cisplatin. (b) Transplatin. Bond lengths are in angstroms. In parentheses are CCSD(T)-calculated free energies (in kcal/mol), where the basis set extension effect on correlation energy is evaluated at the MP2 level. In the free energy, zero point energy, thermal energy, and entropy are included. The sum of 1W_{cis} and one isolated water molecule was taken as energy zero.

geometry optimization. To calculate the solvent radial distribution function, we set a cubic grid of 256 points/axis with the spacing of 0.35 Å. To divide the solvent grid space into three regions, the boundary distances of r_{in} and r_{out} are taken to be 15.0 and 18.0 Å, respectively.

We implemented the present 3D-RISM-SCF method into the GAMESS program code.⁴⁵

4. RESULT AND DISCUSSION

4.1. Geometry and Free Energy Changes in Hydrolyses of Cis- and Transplatin. As the first step of geometry optimization, we investigated the dependence of the geometrical parameters on the computational levels. To this aim, we carried out the DFT calculations with the B3LYP, M06, and M06-2X functionals and the MP2, MP3, and MP4(SDQ) calculations for cis- and transplatin in the gas phase. The geometrical parameters optimized by all these calculations agree well with the experimental values reported by the X-ray analysis,⁴⁶ see the Supporting Information, Table S1. In particular, we found that the DFT calculation with the M06-2X functional provided optimized geometries close to those at the MP4(SDQ) level. Hence, we employed the M06-2X functional for the geometry optimization of the hydrolysis reactions in eqs 1 and 2. The optimized geometrical changes and the free energy profiles in the first and the second

hydrolyses of both cis- and transplatin are shown in Figure 2;⁴⁷ see also the Supporting Information, Figures S1 and S2, for details. For convenience, we denote the reactant system consisting of $\text{PtCl}_2(\text{NH}_3)_2$ (**1**) and one substrate water molecule as **1+W** hereafter, and we use subscripts “cis” and “tr” to represent the species related to cis- and transplatin, respectively.

In the first hydrolysis, the substrate water approaches the square planar Pt complex **1**, to form a hydrogen bond with **1**, which is denoted by **1W**. In both 1W_{cis} and 1W_{tr} , the Ow site of the substrate water approaches the Ha site of NH_3 ligand and the Hw of the substrate water approaches the Cl ligand, which is hereafter denoted as Hw_1 , and the other Hw site of the substrate water is denoted as Hw_2 . When going to the transition state (TS1) from **1W**, the Pt–Cl bond length considerably increases by about 0.40 Å and the Pt complex changes from the square planar to the trigonal bipyramidal structure. After TS1, the Pt–Ow distance becomes shorter to about 2.10 Å and the Pt complex takes a square planar form again; this is denoted by **2Cl**. Though the long Pt–Cl distance (about 3.70 Å) clearly indicates that the Pt–Cl bond is completely broken in both 2Cl_{cis} and 2Cl_{tr} , the Cl anion still remains in the first solvation shell due to the strong Coulombic interaction. Here, we assumed that, in eqs 1 and 2, the Cl anion dissociates from the Pt complex before the second hydrolysis,

Table 1. Solute Energy and Solvation Free Energy Changes in Hydrolysis^a

First Hydrolysis (+Isolated H ₂ O)										
	cisplatin					transplatin				
	1+W	1W	TS1	2Cl	2+Cl ⁻	1+W	1W	TS1	2Cl	2+Cl ⁻
<i>E</i> _{solute}	16.8	0.0	38.4	13.3	121.3	-15.5	-27.8	19.5	6.1	118.9
	(16.7)	(0.0)	(36.4)	(12.4)	(120.1)	(-16.0)	(-28.1)	(16.5)	(4.9)	(116.5)
$\Delta\mu$	-59.9	-44.9	-61.1	-56.3	-156.9	-29.5	-19.1	-44.4	-48.0	-152.4
Second Hydrolysis (+Isolated Cl ⁻)										
	cisplatin					transplatin				
	2+W	2W	TS2	3Cl	3+Cl ⁻	2+W	2W	TS2	3Cl	3+Cl ⁻
<i>E</i> _{solute}	121.3	106.2	150.1	141.4	323.3	118.9	103.6	154.3	144.5	328.8
	(120.1)	(105.0)	(147.1)	(139.6)	(321.1)	(116.5)	(102.0)	(149.6)	(141.9)	(326.0)
$\Delta\mu$	-156.9	-143.9	-165.7	-175.6	-347.2	-152.4	-138.9	-163.2	-172.0	-346.9

^aCalculated at the MP2/BS-II level. In parentheses are energy changes at the CCSD(T)/BS-II level where the basis set extension effect on correlation energy is evaluated at the MP2 level. The sum of 1W_{cis} and one isolated water was taken as energy zero. Unit is kilocalories per mole.

as in previous works by the PCM and the 1D-RISM-SCF-SEDD methods.^{21–24,33} The product of the first hydrolysis, [PtCl(H₂O)(NH₃)₂]⁺ (**2**) and Cl⁻, is denoted by **2+Cl⁻**. The reactant system for the second hydrolysis consists of **2** and one substrate water, which is named **2+W**. The second hydrolysis of **2+W** occurs in a manner similar to that of the first hydrolysis, as shown in Figure 2: one water molecule approaches **2** to form **2W** in which a hydrogen bond is formed between the Cl ligand and the water molecule. Then, the water molecule further approaches the Pt center to afford a trigonal bipyramidal transition state (**TS2**). Finally, the Pt complex takes a square planar geometry in the product (**3Cl**) in which the Cl anion interacts with two water ligands in cisplatin and with one water ligand and one NH₃ ligand in transplatin. The changes of the Pt–Cl and Pt–Ow bond lengths occur in the second hydrolysis in almost the same manner as those in the first hydrolysis.

The free energy profile in the aqueous phase is significantly different from that in the gas phase due to the solvation effects, as shown in Figure 2;⁴⁸ see also the Supporting Information, Figures S1–S3, for details. In the gas phase, the activation free energy in the first hydrolysis was calculated to be 28.8 kcal/mol for cisplatin and 31.8 kcal/mol for transplatin by the CCSD(T) method; see the values in parentheses in Figure S3 in the Supporting Information. This reaction successfully occurs to afford **2Cl** but the Cl dissociation cannot further occur because of the extremely high barrier of the Cl dissociation in both cis- and transplatin (about 110 kcal/mol), as reported in recent work.³³ Also, the reaction energy in this first hydrolysis was calculated to be 8.4 kcal/mol for cisplatin and 17.4 kcal/mol for transplatin, which is defined as the free energy difference between **2Cl** and **1+W**, indicating that the concentration of **2Cl_{tr}** is negligibly small due to the facile backward reaction. In the aqueous phase, however, the activation free energies in the first hydrolysis were calculated to be 20.8 kcal/mol for cisplatin and 20.3 kcal/mol for transplatin,⁴⁹ which are considerably smaller than those in the gas phase. These values are close to the experimental values, 24.1 kcal/mol for cisplatin⁵⁰ and 21.1 kcal/mol for transplatin.⁵¹ Interestingly, the Cl dissociation gives rise to the moderate destabilization of free energy by 5.1 kcal/mol for **2Cl_{cis}** and 5.2 kcal/mol for **2Cl_{tr}** in the aqueous phase, which are much smaller than in the gas phase, as expected. This free energy destabilization for the Cl dissociation is not negligibly small but is much lower than that of the backward reaction of eq 1. In other words, the present 3D-RISM-SCF calculation indicates that (i) the

charged species [PtCl(H₂O)(NH₃)₂]⁺ (**2**) and Cl⁻ are not completely screened by the water solvents, (ii) hence, the Cl dissociation gives rise to a somewhat large free energy increase, but (iii) the solvation effect is indispensable to afford **2**; if the solvation effect was absent, **2** was never formed.

In the second hydrolysis, the activation free energy for **TS2** was calculated to be 20.9 kcal/mol for **2_{cis}** and 23.2 kcal/mol for **2_{tr}**. In cisplatin, the calculated value agrees with the experimental tendency that the second hydrolysis occurs with an activation free energy (23.2 kcal/mol) similar to that of the first hydrolysis (24.1 kcal/mol).⁵⁰ Compared with the very large free energy difference (about 200 kcal/mol) between **3+Cl⁻** and **3Cl** in the gas phase, the corresponding free energy differences in the aqueous phase are significantly small: 7.8 kcal/mol for cisplatin and 8.1 kcal/mol for transplatin. These values are smaller than the activation free energy of the backward reaction of eq 2. Thus, the solvation effect is crucial to afford [Pt(H₂O)₂(NH₃)₂]²⁺ (**3**) by accelerating the dissociation of the substituted Cl anion in both hydrolyses of cis- and transplatin.

Though the geometrical changes and the free energy profiles of cis- and transplatin are similar to each other in the aqueous phase, transplatin becomes less stable than cisplatin after the first and second hydrolyses, as shown in Figure 2. This difference in the free energy profile is clearly reflected in the first and second equilibrium constants, p*K*₁ and p*K*₂. From the free energy difference between **1W** and **2+Cl⁻** at the CCSD(T) level, the equilibrium constant of the first hydrolysis, p*K*₁, was calculated to be 3.74 for cisplatin and 5.94 for transplatin; see the values in parentheses in Figure 2 for the free energies. Also, the p*K*₂ value was calculated to be 6.90 for cisplatin and 9.69 for transplatin. These calculated values agree with the experimental tendency that the equilibrium constant for the second hydrolysis is larger than that for the first hydrolysis in both platin and the hydrolysis of cisplatin occurs more easily than that of transplatin.⁵⁰

4.2. Solute Energy and Solvation Free Energy Changes in Hydrolysis. According to eq 18, we can decompose the MP2 free energy into the solute energy and the solvation free energy, as shown in Table 1. In this decomposition, we found that the free energy components are considerably different between cis- and transplatin in the first hydrolysis but similar to each other in the second hydrolysis. Especially in **1+W**, **1W**, and **TS1**, the solute energy is largely different between the two platin; this difference in the solute

Table 2. Dipole Moment Changes of Solute Molecules by Hydrolysis

	First Hydrolysis									
	cisplatin					transplatin				
	1+W	1W	TS1	2Cl	2+Cl ⁻	1+W	1W	TS1	2Cl	2+Cl ⁻
d ^{aq} ^a	18.3 (2.6) ^c	16.7	18.6	17.2	12.2 (0.0) ^d	0.1 (2.6)	2.6	9.0	12.0	11.7 (0.0)
d ^{gas} ^b	13.6 (2.0)	12.2	13.6	13.1	9.2 (0.0)	0.0 (2.0)	2.0	6.6	10.1	9.1 (0.0)
d ^{aq} - d ^{gas}	4.7 (0.6)	4.5	5.0	4.2	3.0 (0.0)	0.1 (0.6)	0.6	2.4	1.9	2.6 (0.0)
Second Hydrolysis										
	cisplatin					transplatin				
	2+W	2W	TS2	3Cl	3+Cl ⁻	2+W	2W	TS2	3Cl	3+Cl ⁻
	12.2 (2.6) ^c	10.7	14.8	19.9	0.2 (0.0) ^d	11.7 (2.6)	9.2	14.2	19.0	0.0 (0.0)
d ^{aq} ^b	9.2 (2.0)	8.2	10.6	15.8	0.1 (0.0)	9.1 (2.0)	7.2	10.4	15.3	0.0 (0.0)
d ^{aq} - d ^{gas}	3.0 (0.6)	2.5	4.2	4.1	0.1 (0.0)	2.6 (0.6)	2.0	3.8	3.7	0.0 (0.0)

^aCalculated in the aqueous phase. ^bCalculated in the gas phase at aqueous phase geometries. ^cIn parentheses are values for isolated H₂O. Unit is debye. ^dIn parentheses are values for isolated Cl⁻. Unit is debye.

Table 3. Changes of NBO Charges of Solute Molecules in Hydrolysis^a

	First Hydrolysis									
	cisplatin					transplatin				
	1+W	1W	TS1	2Cl	2+Cl ⁻	1+W	1W	TS1	2Cl	2+Cl ⁻
Pt	0.62 (-0.26)	0.62 (-0.24)	0.78 (-0.27)	0.74 (-0.27)	0.74 (-0.23)	0.62 (-0.25)	0.61 (-0.26)	0.79 (-0.25)	0.74 (-0.25)	0.74 (-0.21)
Cl ^(L)	-0.65 (-0.01)	-0.65 (0.00)	-0.65 (0.00)	-0.64 (-0.01)	-0.64 (-0.03)	-0.63 (-0.03)	-0.62 (+0.06)	-0.59 (+0.06)	-0.58 (+0.03)	-0.58 (-0.01)
Cl ^(s)	-0.65 (-0.01)	-0.65 (0.00)	-0.89 (-0.03)	-0.94 (-0.02)	-1.00 (0.00)	-0.63 (-0.03)	-0.62 (+0.04)	-0.89 (-0.02)	-0.94 (-0.02)	-1.00 (0.00)
NH ₃ ^(a)	0.34 (+0.13)	0.33 (+0.11)	0.33 (+0.12)	0.33 (+0.12)	0.34 (+0.09)	0.32 (+0.15)	0.31 (+0.07)	0.31 (+0.08)	0.31 (+0.08)	0.32 (+0.07)
NH ₃	0.34 (+0.13)	0.34 (+0.13)	0.38 (+0.16)	0.38 (+0.14)	0.37 (+0.12)	0.32 (+0.15)	0.32 (+0.09)	0.31 (+0.09)	0.31 (+0.09)	0.31 (+0.10)
H ₂ O ^(s)	0.00 (0.00)	0.01 (0.00)	0.05 (+0.02)	0.14 (+0.04)	0.19 (+0.04)	0.00 (0.00)	0.00 (0.00)	0.07 (+0.04)	0.15 (+0.07)	0.19 (+0.05)
Second Hydrolysis										
	cisplatin					transplatin				
	2+W	2W	TS2	3Cl	3+Cl ⁻	2+W	2W	TS2	3Cl	3+Cl ⁻
	0.74 (-0.23)	0.74 (-0.23)	0.90 (-0.25)	0.87 (-0.26)	0.87 (-0.23)	0.74 (-0.21)	0.74 (-0.21)	0.98 (-0.20)	0.90 (-0.22)	0.90 (-0.23)
Cl ^(s)	-0.64 (-0.03)	-0.65 (-0.02)	-0.89 (-0.06)	-0.89 (-0.05)	-1.00 (0.00)	-0.56 (-0.01)	-0.56 (0.00)	-0.87 (-0.05)	-0.87 (-0.05)	-1.00 (0.00)
NH ₃	0.34 (+0.09)	0.33 (+0.10)	0.38 (+0.11)	0.37 (+0.11)	0.38 (+0.08)	0.32 (+0.07)	0.31 (+0.07)	0.31 (+0.07)	0.31 (+0.06)	0.32 (+0.06)
NH ₃ ^(a)	0.37 (+0.12)	0.37 (+0.10)	0.38 (+0.14)	0.37 (+0.12)	0.38 (+0.08)	0.31 (+0.10)	0.30 (+0.06)	0.31 (+0.08)	0.31 (+0.07)	0.32 (+0.06)
H ₂ O ^(L)	0.19 (+0.04)	0.18 (+0.04)	0.18 (+0.04)	0.14 (+0.04)	0.19 (+0.04)	0.19 (+0.05)	0.19 (+0.08)	0.19 (+0.07)	0.21 (+0.07)	0.23 (+0.05)
H ₂ O ^(s)	0.00 (0.00)	0.03 (+0.01)	0.06 (+0.02)	0.14 (+0.04)	0.19 (+0.04)	0.00 (0.00)	0.02 (0.00)	0.08 (+0.03)	0.14 (+0.07)	0.23 (+0.05)

^a(s), Cl ligand and H₂O molecule participate in hydrolysis; (L), ligand which coordinates with Pt during reaction; (a), NH₃ adjacent to Cl^(s). In parentheses are differences in NBO charges between aqueous phase and gas phase, Q^{aq}_i - Q^{gas}_i, with aqueous phase geometries.

energy is also found in the gas phase, as shown in the Supporting Information, Figure S3. For example, in the aqueous phase, the solute energy, E_{solute} , of $\mathbf{1W}_{\text{cis}}$ is 28.1 kcal/mol less stable than that of $\mathbf{1W}_{\text{tr}}$. On the other hand, the corresponding solvation free energy, $\Delta\mu$, of $\mathbf{1W}_{\text{cis}}$ is 25.8 kcal/mol more stable than that of $\mathbf{1W}_{\text{tr}}$, indicating that the large destabilization of the solute energy of $\mathbf{1W}_{\text{cis}}$ is compensated well by the large stabilization of the solvation free energy. Similarly, due to the solvation effect, the largely destabilizing

solute energies of $\mathbf{1}_{\text{cis}}+\mathbf{W}$ and $\mathbf{TS1}_{\text{cis}}$ are almost compensated by the stabilization of the solvation free energy, too.

We wish to discuss the dipole moment, $|\mathbf{d}|$, of the solute, because it is responsible for the interaction of solute with the surrounding solvent. Actually, the dipole moments of $\mathbf{1}_{\text{cis}}+\mathbf{W}$, $\mathbf{1W}_{\text{cis}}$, and $\mathbf{TS1}_{\text{cis}}$ are much larger than those of $\mathbf{1}_{\text{tr}}+\mathbf{W}$, $\mathbf{1W}_{\text{tr}}$, and $\mathbf{TS1}_{\text{tr}}$, respectively, which agrees with the fact that the solvation free energies of cisplatin-related species are larger than those of transplatin-related species; see Table 2. Also, the

decreasing order of the dipole moment of the solute **TS1_{cis}** (18.6) > **2Cl_{cis}** (17.2) > **1W_{cis}** (16.7) > **2Cl_{tr}** (12.0) > **TS1_{tr}** (9.0) > **1W_{tr}** (2.6) well agrees with the decreasing orders of the stabilizing solvation free energies in the first hydrolysis: $\Delta\mu(\text{TS1}_{\text{cis}}) > \Delta\mu(\text{2Cl}_{\text{cis}}) > \Delta\mu(\text{1W}_{\text{cis}})$ and $\Delta\mu(\text{TS1}_{\text{tr}}) > \Delta\mu(\text{2Cl}_{\text{tr}}) > \Delta\mu(\text{1W}_{\text{tr}})$, where the values in parentheses are dipole moments (in debye); see Tables 1 and 2. These smaller dipole moments in **1_{tr}+W**, **1W_{tr}**, and **TS1_{tr}** are easily understood in terms of the geometry bearing the inversion center.

In the second hydrolysis, the decreasing orders of the dipole moments **2Cl_{cis}** (19.9) > **TS1_{cis}** (14.8) > **1W_{cis}** (11.6) and **2Cl_{tr}** (19.0) > **TS1_{tr}** (14.2) > **1W_{tr}** (9.2) are consistent with the decreasing orders of the stabilization free energies: $\Delta\mu(\text{3Cl}_{\text{cis}}) > \Delta\mu(\text{TS2}_{\text{cis}}) > \Delta\mu(\text{2W}_{\text{cis}})$ and $\Delta\mu(\text{3Cl}_{\text{tr}}) > \Delta\mu(\text{TS2}_{\text{tr}}) > \Delta\mu(\text{2W}_{\text{tr}})$. Interestingly, the solute dipole moment little changes in the first hydrolysis of cisplatin but considerably increases in that of transplatin. However, it similarly changes in the second hydrolyses between cis- and transplatin. This difference will be discussed below again.

To provide clear insight into the change of the solute dipole moment in the hydrolysis, we analyzed the NBO charges on the solute atomic sites.⁵² As shown in Table 3, two important features are observed in the solute charge distribution, as follows: (i) When going from **1W** to **TS1** and from **2W** to **TS2**, the Pt–Cl bond is elongated and the charge transfer occurs from the Pt center to the Cl ligand by about 0.2e in the hydrolyses of both cis- and transplatin. (ii) When going from **TS1** to **2Cl** and from **TS2** to **3Cl**, the Pt–Cl bond is elongated too and the charge transfer occurs from the substrate water to the Pt center by about 0.05e in the hydrolyses of these two isomers. Also, the charge transfer mentioned in (i) increases the polarization of the Pt complexes. Thus, the dipole moments of **TS1** and **TS2** become larger than those of **1W** and **2W**, respectively; $|\delta(\text{TS1})| > |\delta(\text{1W})|$ and $|\delta(\text{TS2})| > |\delta(\text{2W})|$. The Pt–Cl bond elongation usually leads to the increase in the dipole moment because the Cl ligand is negatively charged but the Pt is positively charged, as shown in Table 3; this is consistent with $|\delta(\text{3Cl})| > |\delta(\text{TS2})|$. However, it is not easy to rationalize the reason why the dipole moment of **2Cl_{tr}** becomes larger than that of **TS1_{tr}** but the dipole moment of **2Cl_{cis}** becomes smaller than that of **TS1_{cis}**. This is because two important geometrical changes occur in this reaction stage: One is the Pt–Cl bond elongation, which increases the dipole moment, and the other is the deviation of the Cl position from the $\text{PtCl}(\text{NH}_3)_2$ plane, which decreases the dipole moment of **2Cl_{cis}** and increases the dipole moment of **2Cl_{tr}**. Actually, the Cl–Pt–Cl angle increases from 92 to 122° when going from **TS1_{cis}** to **2Cl_{cis}**. In contrast to the decrease of the Cl–Pt–Cl angle in **2Cl_{tr}**,⁵³ the increase of the Cl–Pt–Cl angle reduces the total dipole moment of **2Cl_{cis}** despite the Pt–Cl bond elongation from **TS1_{cis}**, leading to the complicated order of the solvation free energies of cisplatin-related species, as mentioned above: $\Delta\mu(\text{TS1}_{\text{cis}}) > \Delta\mu(\text{2Cl}_{\text{cis}}) > \Delta\mu(\text{1W}_{\text{cis}})$.

4.3. Solvent Configurational Change in Hydrolysis.

When going from **1** to **3**, the solvent configurational changes occur around the Pt center, as shown in Figure 3. In the solvation structure of **1**, we found that some of the water solvent exists near the Pt center in the Hw-interacting orientation, where the Hw site of water solvent rather than the Ow site of water solvent approaches the Pt center; see probability densities at about 3.0 Å in Figure 3. In **2** and **3**, on the other hand, the probability density of the Hw site

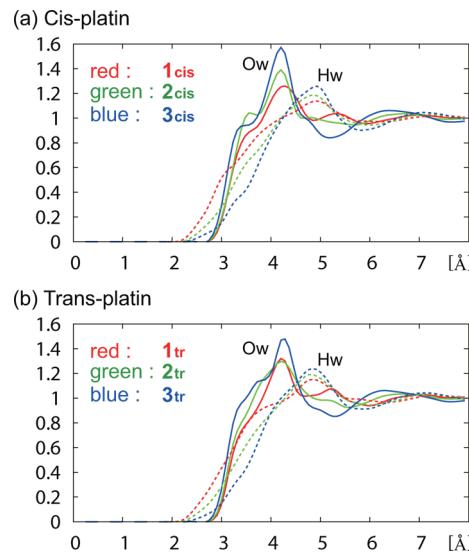


Figure 3. Solvent radial distribution function around Pt center in hydrolyses of cis- and transplatin. Solid line represents solvent Ow, and dashed line represents solvent Hw. Red, green, and blue lines are **1**, **2**, and **3**, respectively.

apparently decreases around 3.0 Å, indicating that the Ow-interacting configuration becomes preferable to the Hw-interacting one. Especially in **3**, the first solvation shell around the Pt center is mainly composed of the Ow-interacting water solvents around 4.2 Å. Actually, when going from **1** to **3**, the Ow-interacting water molecules are found to increase not only in the first solvation shell but also in a more distant region from the Pt center, as shown in the Supporting Information, Figure S4; the latter is induced by the positive net charge of the Pt complex through the long-range Coulombic interaction. Note that the position of the first solvation peak of the Ow-interacting water (about 4.2 Å) is somewhat distant from the Pt center. This result clearly indicates that most of the water solvents in the first solvation shell do not directly interact but indirectly interact with the Pt center through the hydrogen bonds with the ligands of the Pt complex, as discussed below.

To clarify where the Hw- and the Ow-interacting waters dominantly exist near the solute, we examined how the solvation structure around the ligands changes along the hydrolysis of **1** to **3**. The solvent radial distribution function of Figure S5 in the Supporting Information indicates that the Hw-interacting configuration is found in the region near the Cl ligand through the Cl–Hw hydrogen bond (about 2.2 Å) and the Ow-interacting one is found in the region near the NH_3^+ ligand through the $\text{H}_3\text{N}^+–\text{Ow}$ hydrogen bond (about 2.0 Å); see Figure 4a–c for the schematic picture. Also, in the region near the H_2O ligand coordinated with the Pt center, the Ow-interacting configuration is displayed by the Hw–Ow distance of about 1.8 Å (Figure S5 in the Supporting Information), which corresponds to the usual hydrogen bond distance (Figure 4c). In particular, it is indicated that the substitution of the Cl ligand for the water molecule induces not only the change of the global solvation structure around the Pt complex (see Figure S4 in the Supporting Information) but also that of the local solvation structure around the H_2O ligand from the Hw-interacting configuration to the Ow-interacting one. These changes in solvation structure occur to increase the stabilization by the Coulombic interaction; remember that the net charge of the Pt complex becomes positive in the reaction.

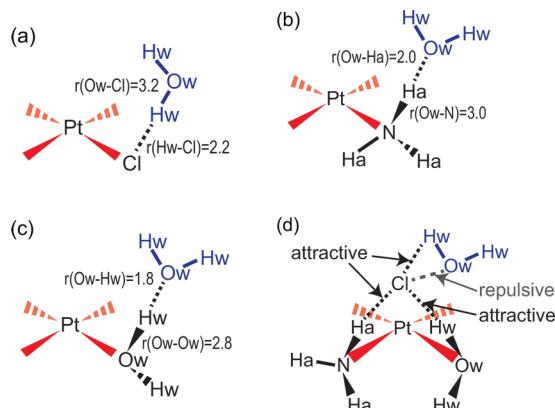


Figure 4. Hydrogen bonding structure between water solvent and ligand and interaction between water solvent and Cl counteranion. Hydrogen bonds between water solvent and (a) Cl, (b) NH₃, and (c) H₂O ligand, respectively. Unit is angstroms. (d) Interaction between water solvent and Cl anion.

To investigate the solvent configurational changes around the solute when passing through TS1 and TS2, the solvent radial distribution functions around the Pt center and the ligands are shown in the Supporting Information, Figures S6 and S7. Figures S6 and S7 show that the first solvation shell around the Pt center changes in both isomers in a somewhat complicated manner. This is because the cavity is considerably changed by substituting the Cl ligand for water when going from 1W to 2Cl and from 2W to 3Cl. However, one clear and characteristic change is observed around the ligands, especially in the region near the Cl ligand substitution; in this region, Hw-interacting water solvents largely increase when going from 1W to TS1 and from 2W to TS2 but change little when going from TS1 to 2Cl and from TS2 to 3Cl.

When going from 2Cl to 2+Cl⁻ and from 3Cl to 3+Cl⁻, the Cl anion dissociates from the Pt complex. In this process, the Hw-interacting water solvents largely increase near the dissociating Cl anion because the short-range Coulombic attractive interaction with the Cl anion increases but the LJ and long-range Coulombic repulsive interactions with the Pt

complex decrease along the dissociation of the Cl anion. Another characteristic change of the solvent configuration occurs around the substrate water. When going from 1W to 2+Cl⁻, the Ow-interacting water, which directly interacts with the Hw₁ site of the substrate water through the Ow–Hw hydrogen bond (about 1.8 Å), does not monotonically increase but considerably decreases in 2Cl, because the Cl counteranion prefers the Hw-interacting water and prevents the Ow-interacting water from solvating the Hw₁ site due to the strong Coulombic repulsion; see Figure 4d. Actually, this characteristic solvation change around the Hw₁ site is similarly observed in the second hydrolysis, as shown in Figure S7 in the Supporting Information. It is important to understand how these solvent configurational changes influence the solvation free energy profiles of the hydrolysis, as will be discussed in section 4.4.

4.4. Energy Decomposition Analysis of Intermolecular Interaction.

To present microscopic insight into the solvation free energy, $\Delta\mu$, in Table 1, we examined the spatial distribution function (SDF) of solvation free energy, $\Delta\mu_{\text{SDF}}(\mathbf{r})$, which is defined by eq 28:

$$\Delta\mu_{\text{SDF}}(\mathbf{r}) = \frac{\rho^V}{\beta} \sum_{\xi} \left[\frac{1}{2} h_{\xi}^{-2}(\mathbf{r}) \Theta(-h_{\xi}(\mathbf{r})) - c_{\xi}(\mathbf{r}) \right. \\ \left. - h_{\xi}(\mathbf{r}) c_{\xi}(\mathbf{r}) \right] \quad (28)$$

Note that the integration of $\Delta\mu_{\text{SDF}}(\mathbf{r})$ over the entire 3D grid space corresponds to the solvation free energy, $\Delta\mu$, in eq 20. Using eq 28, we can display the spatial distribution of the solvation free energy, as shown in Figure 5. When the first hydrolysis occurs from 1W to 2Cl, the stabilizing region of the solvation free energy (blue region in Figure 5a) largely increases around the substituted Cl ligand in both cis- and transplatin. Also, the stabilizing and destabilizing regions of the solvation free energy in 1W_{tr} are apparently much smaller than that in 1W_{cis}, reflecting the small dipole moment of 1W_{tr}. In the second hydrolysis going from 2W to 3Cl, however, the stabilizing region does not change significantly, as seen in Figure 5b. One of the important differences between the first and the second hydrolyses is that the stabilization around the

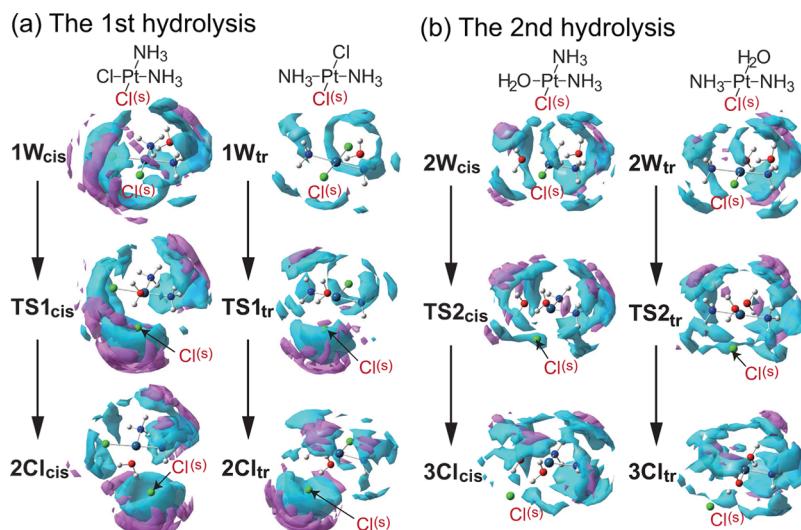


Figure 5. Spatial distribution changes of solvation free energy in the first and second hydrolyses. (a) First hydrolysis. (b) Second hydrolysis. Blue region is stabilized, and purple region is destabilized. Surface is plotted by (a) $\Delta\mu_{\text{SDF}}(\mathbf{r}) = 0.8 \text{ kcal}/(\text{mol}\cdot\text{\AA}^3)$ and (b) $\Delta\mu_{\text{SDF}}(\mathbf{r}) = 2.4 \text{ kcal}/(\text{mol}\cdot\text{\AA}^3)$.

Table 4. Linear Response Solvation Free Energy Components in Hydrolysis^a

	First Hydrolysis					transplatin				
	1+W	1W	TS1	2Cl	2+Cl ⁻	1+W	1W	TS1	2Cl	2+Cl ⁻
total	-78.1	-64.1	-81.9	-77.3	-179.5	-49.0	-37.8	-61.4	-68.9	-174.6
Cl ^(s)	-18.5	-17.9	-37.8	-41.0	-97.2	-10.9	-11.1	-30.4	-39.3	-97.2
H ₂ O ^(s)	-11.6	-5.2	-1.4	1.9	-18.4	-11.6	-7.4	-6.2	-4.4	-26.2
other ^b	-48.0	-41.0	-42.7	-38.2	-63.9	-26.5	-19.3	-24.8	-25.2	-61.2
Pt	-2.0	-2.1	0.0	-1.8	-6.6	-1.2	-1.1	0.0	-2.0	-5.4
Cl ^(L)	-18.5	-15.3	-16.7	-10.8	4.8	-10.9	-8.2	-10.9	-8.3	4.4
NH ₃ ^(a)	-13.7	-10.9	-12.0	-10.9	-34.1	-7.2	-3.5	-5.8	-4.9	-25.1
NH ₃	-13.8	-13.7	-14.0	-14.7	-28.0	-7.2	-7.5	-8.1	-10.0	-25.0
total + H ₂ O	-89.7	-75.7	-93.5	-88.9	-191.1	-60.6	-49.4	-73.0	-80.5	-186.2
Second Hydrolysis										
	cisplatin					transplatin				
	2+W	2W	TS2	3Cl	3+Cl ⁻	2+W	2W	TS2	3Cl	3+Cl ⁻
total	-93.9	-79.7	-103.7	-113.3	-287.6	-89.0	-77.2	-101.0	-109.9	-286.4
Cl ^(s)	4.8	5.8	-1.9	-7.3	-97.2	4.4	4.6	-1.2	-8.2	-97.2
H ₂ O ^(s)	-11.6	-5.0	-7.6	-10.7	-32.5	-11.6	-5.8	-9.7	-11.1	-39.5
other ^b	-87.1	-80.5	-94.2	-95.3	-157.9	-81.8	-76.0	-90.1	-90.6	-149.7
Pt	-6.6	-3.8	-21.8	-15.2	-25.1	-5.4	-4.8	-24.6	-15.0	-28.5
NH ₃	-34.1	-34.2	-28.7	-34.3	-49.9	-25.1	-24.4	-22.8	-28.1	-41.5
NH ₃ ^(a)	-28.0	-24.4	-26.5	-33.8	-48.9	-25.0	-21.4	-20.0	-21.0	-41.5
H ₂ O ^(L)	-18.4	-18.1	-17.2	-12.0	-32.8	-26.2	-25.5	-22.6	-26.5	-39.5
total + Cl ⁻	-191.1	-176.9	-200.9	-210.5	-384.8	-186.2	-174.4	-198.2	-207.1	-383.6

^aCalculated at the MP2/BS-II level. (s), Cl ligand and H₂O molecule participate in hydrolysis; (L), ligand which coordinates with Pt during reaction; (a), NH₃ adjacent to Cl^(s). ^bSum of remaining moieties of Pt complex. Unit is kilocalories per mole.

substituted Cl ligand drastically occurs in the first hydrolysis but does not occur in the second hydrolysis in both cis- and transplatin.

To provide detailed insight into the solvation free energy changes by the hydrolysis, we investigated the solute–solvent interaction energy by the energy decomposition analysis based on the point charge approximation:

$$\begin{aligned} E_{\text{int}}^{\text{UV}} &= \sum_{\xi} \int d\mathbf{r} g_{\xi}(\mathbf{r}) (u_{\xi}^{\text{ES}(e)}(\mathbf{r}) + u_{\xi}^{\text{ES}(n)}(\mathbf{r}) + u_{\xi}^{\text{LJ}}(\mathbf{r})) \\ &\approx \sum_{b,\xi} \int d\mathbf{r} g_{\xi}(\mathbf{r}) \left[\frac{q_{\xi}^V(Q_b + Z_b)}{|\mathbf{r} - \mathbf{R}_b|} \right. \\ &\quad \left. + 4\epsilon_{b\xi} \left\{ \left(\frac{\sigma_{b\xi}}{|\mathbf{r} - \mathbf{R}_b|} \right)^{12} - \left(\frac{\sigma_{b\xi}}{|\mathbf{r} - \mathbf{R}_b|} \right)^6 \right\} \right] \end{aligned} \quad (29)$$

where $g_{\xi}(\mathbf{r})$ is obtained by the 3D-RISM-RHF method. According to the linear response theory,^{54–56} the solvation free energy mostly changes in parallel with half of the average solute–solvent interaction energy. The linear response solvation free energy was used to elucidate the nonequilibrium free energy in the previous works with the 1D-RISM-SCF method.^{57–60} We employed here the linear response approximation (LRA) to analyze the solvation free energy profiles with $\Delta\mu_b^{\text{LRA}}$, which is half of $E_{\text{int}}^{\text{UV}}$.

Here, we separated the total system into three moieties: the Cl ligand moiety substituted in the reaction, the water molecule approaching the Pt, and the remaining moiety of the Pt complex. When going from 1W to 2Cl in the first hydrolyses of cis- and transplatin, the increase of the stabilization energy,

$\Delta\mu_b^{\text{LRA}}$, is mainly attributed to the substituted Cl ligand moiety, as shown in Table 4. On the other hand, the sum of the stabilization energies, $\Delta\mu_b^{\text{LRA}}$, on the water molecule and the remaining moieties of the Pt complex decreases in cisplatin but changes little in transplatin. In the next step which is the Cl dissociation going from 2Cl to 2+Cl⁻, however, the stabilization of the solvation free energy increases around the Pt complex by about 50 kcal/mol and around the leaving Cl anion by about 56 kcal/mol. In the Pt complex moiety, the H₂O ligand and two NH₃ ligands contribute to the stabilization of the solvation free energy, though the Cl ligand gives rise to destabilization somewhat. These solvation free energy changes are reasonably interpreted by considering that 2+Cl⁻ contains the ionic [PtCl(H₂O)(NH₃)₂]⁺ (2) with the positive net charge, as follows: the positively charged [PtCl(H₂O)(NH₃)₂]⁺ moiety is very favorable for the Ow-interacting configuration of water solvents, as discussed in section 4.3. The Ha sites of the NH₃ ligand and the Hw sites of the H₂O ligand are suitable for the hydrogen bond with the Ow sites of the water solvents, which leads to the large stabilization energy by solvation, as discussed above. On the other hand, the coordinating Cl ligand bearing the negative charge is repulsive with the Ow-interacting configuration through the Coulombic interaction, as discussed above, which leads to the free energy destabilization. The main difference in the solvation free energy between cis- and transplatin is found on the Pt complex moieties of 1W, TS1, and 2Cl; all the ligands and Pt center in cisplatin are more stabilized by the water solvents than in transplatin except for the substrate water.

In the second hydrolysis, the stabilization of the solvation free energy around the substituted Cl ligand moiety is much smaller than that around the Pt complex moiety, as depicted in Figure Sb. Though the solvation free energy around the

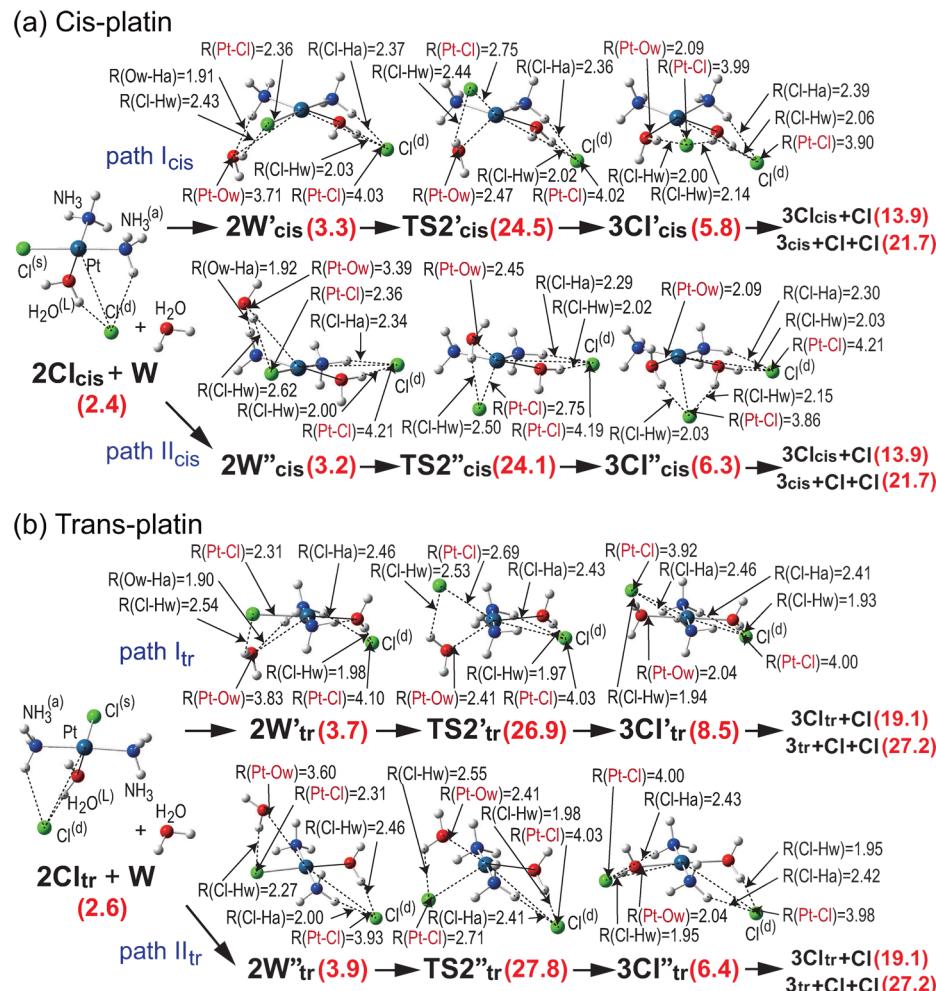


Figure 6. Geometry and CCSD(T)-calculated free energy changes in the second hydrolysis with Cl counteranion in the first solvation shell. (a) Cisplatin. (b) Transplatin. Bond lengths are in angstroms. In parentheses are CCSD(T)-calculated free energies (in kcal/mol), where the basis set extension effect on correlation energy is evaluated at the MP2 level. In the free energy, zero point energy, thermal energy, and entropy are included. The sum of $1\mathbf{W}_{\text{cis}}$ and one isolated water molecule was taken as energy zero.

substituted Cl ligand accelerates less the second hydrolysis than the first hydrolysis, the solvation free energy around the Pt complex moiety contributes more to the second hydrolysis. When going from $2\mathbf{W}$ to $\mathbf{TS}2$, the stabilization energy around the Pt center increases, because of two factors: one is the charge transfer from the Pt center to the substituted Cl ligand (about $0.2e$) and the other is the increase in Ow-interacting water molecules around the Pt center in the second hydrolysis. In the next step in which the Cl dissociation process occurs from $3\mathbf{Cl}$ to $3+\mathbf{Cl}^-$, the stabilization of the solvation free energy around the leaving Cl anion moiety increases by about 90 kcal/mol like that on the Pt complex moiety. In this dissociation process, all the ligands and the Pt center contribute to the stabilization of the solvation free energy, because the Pt center, H_2O , and NH_3 ligands of 3 are favorable for the Ow-interacting configuration, as discussed in section 4.3. These changes of the solvation free energy occur in the second hydrolysis reactions of cis- and transplatin.

4.5. Second Hydrolysis with Substituted Cl Anion in the First Solvation Shell. In sections 4.1–4.4, the free energy profile of the second hydrolysis was calculated under the assumption that the substituted Cl anion dissociates from the Pt complex prior to the second hydrolysis, because this assumption was tacitly employed in previous theoretical

works.^{21–24,33} As shown in Figure 2, however, the free energy profiles of both cis- and transplatin indicate that the Cl anion substituted by the first hydrolysis wants to stay as a counteranion in the first solvation shell of $3\mathbf{Cl}$ due to the strong Coulombic attraction between the positively charged 2 and the negatively charged \mathbf{Cl}^- . This result suggests that the second hydrolysis occurs in the presence of the Cl counteranion in the first solvation shell. Considering this possibility, we theoretically investigated the second hydrolysis with keeping the Cl counteranion in the first solvation shell of $2\mathbf{Cl}$, as shown in Figure 6; see also the Supporting Information, Figures S8 and S9, for details. Note that we considered here two types of the reaction paths I and II, because the upper molecular plane of the square planar Pt complex, $[\text{PtCl}(\text{H}_2\text{O})(\text{NH}_3)_2]^+$, is not equivalent to the lower plane due to the presence of Cl anion and a water molecule can approach the Pt complex from both sides of the molecular plane.

Despite the presence of the Cl counteranion in the first solvation shell, the second hydrolysis can occur through the trigonal bipyramidal transition state, $\mathbf{TS}2'$ (or $\mathbf{TS}2''$), which resembles $\mathbf{TS}2$; see Figure 6. Hereafter, the primes “'” and “''” such as in \mathbf{TS}' and \mathbf{TS}'' represent the reaction species with the Cl counteranion in the first solvation shell, where a single prime means the species in path I and a double prime means

Table 5. Energy Components in the Second Hydrolysis with Cl Counteranion in the First Solvation Shell^a

	cisplatin						transplatin					
	2W'	TS2'	3Cl'	2W"	TS2"	3Cl"	2W'	TS2'	3Cl'	2W"	TS2"	3Cl"
(A) Solute Energy and Solvation Free Energy												
E_{solute}	-3.0 (-3.9)	36.8 (34.1)	28.9 (27.5)	-2.8 (-3.7)	36.4 (33.6)	29.6 (28.1)	-6.8 (-8.0)	35.3 (31.2)	17.3 (15.5)	-4.0 (-5.2)	44.0 (39.8)	20.4 (18.6)
$\Delta\mu$	-41.7	-59.0	-71.2	-41.7	-58.8	-71.6	-36.7	-53.4	-56.1	-39.3	-60.7	-61.2
(B) Linear Response Solvation Free Energy Components												
total	-70.7	-89.8	-101.5	-70.2	-88.9	-101.6	-64.2	-82.1	-85.7	-68.7	-89.4	-90.3
Cl ^(s)	-7.2	-25.3	-38.0	-8.5	-25.5	-38.2	-5.9	-22.6	-28.6	-5.2	-25.6	-30.9
H ₂ O ^(s)	-5.4	-3.3	-2.2	-4.4	-3.6	-2.4	-6.9	-6.5	-4.1	-8.7	-6.6	-4.2
other ^b	-58.1	-61.2	-61.3	-57.3	-59.8	-61.0	-51.4	-53.0	-53.0	-54.7	-57.2	-55.2
Pt	-1.5	-3.3	-3.2	-1.5	-4.0	-4.9	-2.0	-3.7	-4.7	-2.1	-3.9	-3.8
Cl ^(d)	-36.4	-34.4	-33.2	-36.7	-35.0	-33.3	-36.5	-33.8	-28.7	-36.6	-37.4	-30.8
NH ₃	-11.8	-14.2	-21.5	-12.5	-15.2	-20.8	0.7	-2.6	-7.6	-3.4	-2.3	-8.1
NH ₃ ^(a)	-9.6	-8.1	-11.3	-8.1	-7.6	-9.9	-11.6	-11.7	-8.5	-10.2	-11.7	-8.4
H ₂ O ^(L)	1.2	-1.2	6.9	1.5	2.0	7.9	-2.0	-1.2	-3.5	-2.5	-1.9	-4.1

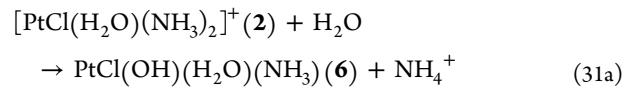
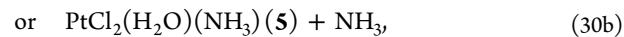
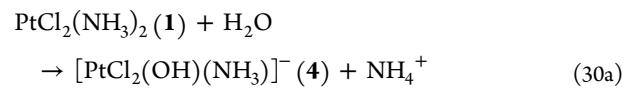
^aCalculated at the MP2/BS-II level. (s), Cl ligand and H₂O molecule participate in hydrolysis.(L), ligand which coordinates with Pt during reaction. (d), Cl anion substituted in first hydrolysis. (a), NH₃ adjacent to Cl^(d) anion. ^bSum of remaining moieties of Pt complex. In parentheses are energy changes at the CCSD(T)/BS-II level where the basis set extension effect on correlation energy is evaluated at the MP2 level. The sum of 1W_{cis} and one isolated H₂O was taken as energy zero. Unit is kilocalories per mole.

the species in path II. In particular, the Pt–Cl and Pt–Ow bond lengths of TS2' and TS2" agree with those of TS2 within 0.04 Å in both monoqua 2_{cis} and 2_{tr}. Though these coordinate bond lengths are not sensitive to the presence of the Cl anion in the first solvation shell, the hydrogen bonding structure is somewhat influenced by the Cl anion. This is because the orientations of Ha–N bonds of the NH₃ ligand and Hw–Ow bonds of the H₂O ligand are influenced by the Cl counteranion through the hydrogen bond, as shown in Figure 4d. Accordingly, the Pt–Ow distance is different among 2W, 2W', and 2W" and the Pt–Cl distance is also different among the 3Cl, 3Cl', and 3Cl"; a comparison of free energies among 3Cl, 3Cl', and 3Cl" clearly indicates that the Cl anion favorably stays in the first solvation shell distant from the Pt center by about 4 Å, as shown in Figure 6. The activation free energy of this hydrolysis was calculated to be 21.2 kcal/mol for path I and 20.9 kcal/mol for path II in cisplatin and 23.2 kcal/mol for path I and 23.9 kcal/mol for path II in transplatin; see Figure 6. Comparison with the activation free energy of TS2 without the Cl counteranion (see section 4.1; 20.9 kcal/mol for cisplatin and 23.2 kcal/mol for transplatin), leads to conclusions that the activation free energy of the second hydrolysis depends little on the presence of the Cl counteranion in the first solvation shell but the endothermicity of the hydrolysis decreases in both isomers by the presence of the Cl counteranion in the first solvation shell. Judging from the fact that TS2' and TS2" are lower in free energy than TS2, it is concluded that the second hydrolyses of cis- and transplatin dominantly occur without the dissociation of the Cl counteranion from the first solvation shell.⁶¹ This suggestion leads to the expectation that the second hydrolysis is accelerated in the solution with high ionic strength.

To examine the reason why the solvation is influenced by the Cl counteranion in the first solvation shell, we calculated the free energy components on reaction paths I and II. Table 5 clearly shows two features of the solute energy and the solvation free energy, as follows: If the Cl anion does not dissociate from monoqua 2, the absolute value of the solvation free energy becomes much smaller throughout the second hydrolysis, and the free energy components, E_{solute} and $\Delta\mu$, in

3Cl' and 3Cl" change in a different manner between 2_{cis} and 2_{tr}. The former feature arises from the neutral charge of the whole solute, 2Cl. The latter feature arises from the geometrical features that 3Cl'_{tr} and 3Cl"_{tr} take a structure so as to decrease the repulsive interaction between two Cl anions and 3Cl'_{cis} and 3Cl"_{cis} take a structure so as to increase the hydrogen bonding interaction between the solute and the water solvents; see 3Cl'_{cis}, 3Cl'_{tr}, etc. in Figure 6. Also, we found that when going from 2W' to 3Cl' and from 2W" to 3Cl", the stabilizing solvation free energy is dominantly observed around the Cl ligand moiety; see Cl^(s) in Table 5. This is because the Ow-interacting configuration around the Pt complex moiety is not favorable for the Cl counteranion in the first solvation shell but the Pt–Cl bond elongation weakens this unfavorable situation; see Figure 4d. Actually, when the second hydrolysis occurs with keeping the Cl counteranion in the first solvation shell, the Pt center contributes little to the stabilization of the solvation free energy in a manner similar to that for the first hydrolyses of cis- and transplatin, as shown in Table 5. On the other hand, when going from 2W' to 3Cl' and from 2W" to 3Cl", the presence of the Cl counteranion suppresses the destabilization of the E_{solute} energy due to the Coulombic interaction, which leads to the decrease in the endothermicity in the second hydrolysis; see E_{solute} terms of 2W, 3Cl, and these related species in Tables 1 and 5.

4.6. Other Substitution Reaction of NH₃ Ligand for Water Solvent. One of the other possible reactions of cis- and transplatin in aqueous phase is the substitution reaction of the NH₃ ligand for the water solvent, as shown in eqs 30a, 30b and 31a, 31b.



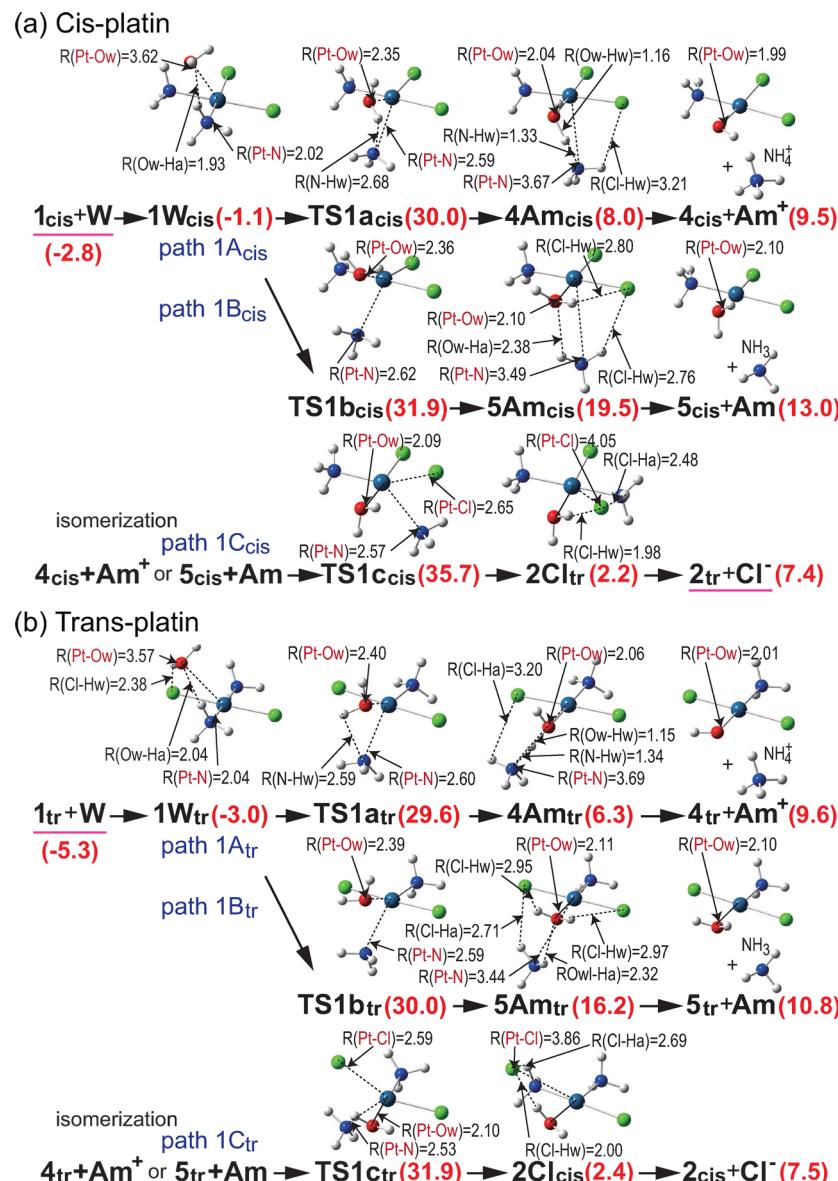
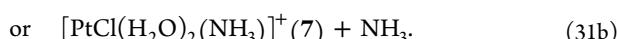


Figure 7. Geometry and CCSD(T)-calculated free energy changes of $\mathbf{1}_{\text{cis}}$ and $\mathbf{1}_{\text{tr}}$ in substitution of NH_3 ligand for water molecule. (a) Cisplatin. (b) Transplatin. Bond lengths are in angstroms. In parentheses are CCSD(T)-calculated free energies (in kcal/mol), where the basis set extension effect on correlation energy is evaluated at the MP2 level. In the free energy, zero point energy, thermal energy, and entropy are included. The sum of $\mathbf{1}\mathbf{W}_{\text{cis}}$ and one isolated water molecule was taken as energy zero.



The geometrical changes and the free energy profiles of eqs 30a and 30b are calculated with the 3D-RISM-SCF method, as shown in Figure 7; see also Supporting Information, Figures S10 and S11, for details. Those of eqs 31a and 31b are shown in Supporting Information, Figures S12 and S13. For convenience, we hereafter denote $[\text{PtCl}_2(\text{OH})(\text{NH}_3)]^-$ as $\mathbf{4}$, $\text{PtCl}_2(\text{H}_2\text{O})(\text{NH}_3)$ as $\mathbf{5}$, $\text{PtCl}(\text{OH})(\text{H}_2\text{O})(\text{NH}_3)$ as $\mathbf{6}$, and $[\text{PtCl}(\text{H}_2\text{O})_2(\text{NH}_3)]^+$ as $\mathbf{7}$. If the substitution of the Cl ligand for NH_3 occurs in *trans*- $\text{PtCl}_2(\text{H}_2\text{O})(\text{NH}_3)$ ($\mathbf{5}_{\text{tr}}$), *cis*- $[\text{PtCl}(\text{H}_2\text{O})(\text{NH}_3)_2]^+$ ($\mathbf{2}_{\text{cis}}$) is formed. Also, if the substitution of the Cl ligand for NH_3 occurs in *trans*- $[\text{PtCl}(\text{H}_2\text{O})_2(\text{NH}_3)]^+$ ($\mathbf{7}_{\text{tr}}$), *cis*- $[\text{Pt}(\text{H}_2\text{O})_2(\text{NH}_3)_2]^{2+}$ ($\mathbf{3}_{\text{cis}}$) is formed. Hence, these reactions are important in the chemistry of cisplatin.

In eq 30, the substitution of the NH_3 ligand for the water molecule occurs via two different reaction paths, 1A and 1B, as

follows: In path 1A, one water molecule reacts with $\mathbf{1}$ to afford $\mathbf{4Am}$ through the trigonal bipyramidal transition state TS1a in which the water molecule forms a hydrogen bond with the NH_3 ligand; see Figure 7a. In $\mathbf{4Am}$, one $\text{Hw}-\text{Ow}$ bond length of the substrate water is elongated to 1.16 \AA in the *cis* isomer and 1.15 \AA in the *trans* isomer. In path 1B, one water molecule reacts with $\mathbf{1}$ to afford $\mathbf{5Am}$ through the trigonal bipyramidal transition state TS1b in which no hydrogen bond is formed between the water and the NH_3 ligand; see Figure 7b. In $\mathbf{5Am}$, two $\text{Hw}-\text{Ow}$ bond lengths of the substrate water change little. Judging from the $\text{Hw}-\text{Ow}$ bond lengths of the substrate waters in $\mathbf{4Am}$ and $\mathbf{5Am}$, the dissociation of NH_3 leads to the formation of $\mathbf{4}$ and NH_3^+ (denoted by $\mathbf{4}+\text{Am}^+$) in path 1A and the formation of $\mathbf{5}$ and NH_3 (denoted by $\mathbf{5}+\text{Am}$) in path 1B.

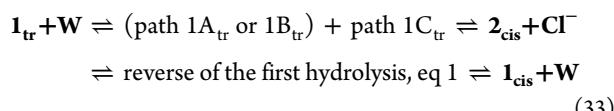
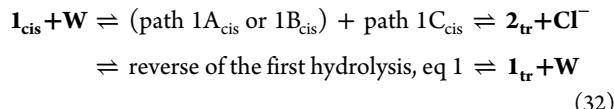
As shown in Figure 7, the activation free energy was calculated to be 31.1 kcal/mol for path 1A_{cis} and 33.0 kcal/mol for path 1B_{cis}, which is about 10 kcal/mol higher than that of

the substitution of the Cl ligand for the water solvent in the first hydrolysis, eq 1 (20.8 kcal/mol for cisplatin). Also, the activation free energy was calculated to be 32.6 kcal/mol for path 1A_{tr} and 33.0 kcal/mol for path 1B_{tr}, which is about 12 kcal/mol higher than that of the substitution of the Cl ligand for the water solvent in the first hydrolysis, eq 1 (20.3 kcal/mol for transplatin). These larger free energy barriers in eqs 30a and 30b indicate that the substitution of the NH₃ ligand for the water molecule occurs much slower than that of the Cl ligand for the water solvent. Though the dissociation of NH₃ from **5Am** readily affords **5+Am** without the free energy barrier, **4Am** is much more stable than **5Am**, as shown in Figure 7, indicating that the substituted NH₃ ligand in path 1A tends to stay favorably in the first solvation shell as ammonium cation NH₄⁺.

If the substituted NH₃ ligand in **4Am** or **5Am** reacts with the Cl ligand again, the cis-trans isomerization product **2** is produced through a trigonal bipyramidal transition state **TS1c**; see path 1C in Figure 7. To induce the cis-trans isomerization from **1** to **2**, the substituted NH₃ ligand needs to migrate from the H₂O to the Cl ligand and the substitution of the Cl ligand for NH₃ must occur through transition state **TS1c**. This activation free energy for **TS1c** is much higher than those of the dissociations of NH₃ and NH₄⁺, suggesting that this reaction starts from **4+Am** or **5+Am**, respectively. The stepwise reactions of **1** to **2** through either paths 1A and 1C or paths 1B and 1C need large activation free energy, 31.1 kcal/mol for **TS1a_{cis}**, 32.6 kcal/mol for **TS1a_{tr}**, 33.0 kcal/mol for **TS1b_{cis}**, and 33.0 kcal/mol for **TS1b_{tr}**, as mentioned above. In the reverse reactions from **2** to **1**, the activation free energy is 33.5 kcal/mol for **TS1c_{cis}** and 29.5 kcal/mol for **TS1c_{tr}**. These values suggest that the cis \rightleftharpoons trans isomerization via either paths 1A and 1C or paths 1B and 1C cannot be ruled out in the chemistry of cisplatin.

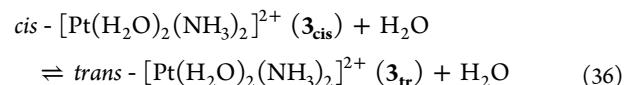
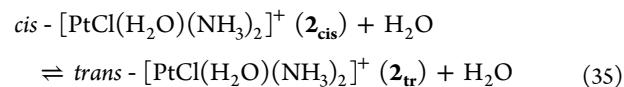
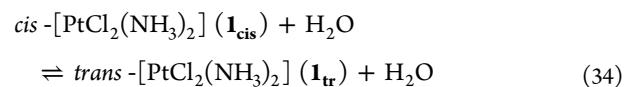
In eq 31, the substitution of the NH₃ ligand for the water molecule leads to [PtCl(H₂O)(NH₃)(OH)...HNH₃]⁺ (**6Am**) through a trigonal bipyramidal transition state **TS2a** (path 2A) in which the water molecule forms a hydrogen bond with the NH₃ ligand; see the Supporting Information, Figures S12 and S13. In **6Am**, one Ow-Hw bond of the substrate water is elongated to 1.50 Å in the cis isomer and 1.15 Å in the trans isomer. The activation free energy was calculated to be 35.9 kcal/mol for path 2A_{cis} and 32.2 kcal/mol for path 2A_{tr}; these values are larger than those of the substitution of the Cl ligand for the water molecule in the second hydrolysis, eq 2 (20.9 kcal/mol for cisplatin and 23.2 kcal/mol for transplatin); see the Supporting Information, page S4, for details. Also, **TS2a** and **TS2c** are much higher in free energy than **TS1a**, **TS1b**, and **TS1c**, suggesting that the cis-trans isomerization through **6Am** is not important here, as shown in the Supporting Information, page S4.

The above results lead to the conclusion that eqs 32 and 33 participate in the cis \rightarrow trans and trans \rightarrow cis isomerizations.



We wish to mention here that the reverse reaction of eq 1 does not necessarily occur in the forward reactions of eqs 32 and 33 and the cis-trans isomerization product **2** can afford **3** through the usual hydrolyses, eq 2. The forward reaction of eq 32 needs the activation free energy of 31.1 kcal/mol for path 1A_{cis} and 33.0 kcal/mol for path 1B_{cis}, and the backward reaction of eq 32 needs the activation free energy of 33.5 kcal/mol for path 1C_{cis}. The forward reaction of eq 33 needs the activation free energy of 32.6 kcal/mol for path 1A_{tr} and 33.0 kcal/mol for path 1B_{tr}, and the backward reaction of eq 33 needs the activation free energy of 29.5 kcal/mol for path 1C_{tr}. These values are considerably larger than those of usual hydrolyses by eqs 1 and 2, but they do not mean that these reactions never occur. Hence, these results suggest that the hydrolysis of **1** must be performed under mild conditions, because the cis \rightarrow trans isomerization (backward reaction of eq 33) occurs earlier than the trans \rightarrow cis isomerization (forward reaction of eq 33).

4.7. Possibility of Other Cis-Trans Isomerization Reactions. We also investigated the cis-trans isomerization reactions with the water solvent via Berry's pseudorotation,⁶² as follows:



However, we could not find any stable trigonal bipyramidal five-coordinate Pt(II) complex in eqs 34–36, which is a key intermediate in Berry's pseudorotation; see the Supporting Information, page S5, for details.

Then, we investigated a single-step cis-trans isomerization and optimized the geometries of the transition states, **TS_{2cis/2tr}** and **TS_{3cis/3tr}**, with the 3D-RISM-SCF method, as shown in Figure 8; note that any single-step isomerization via H₂O

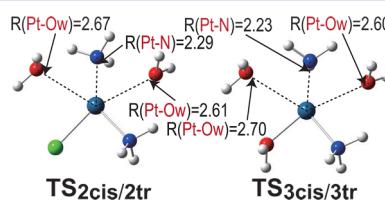
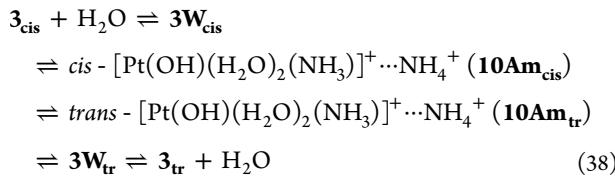
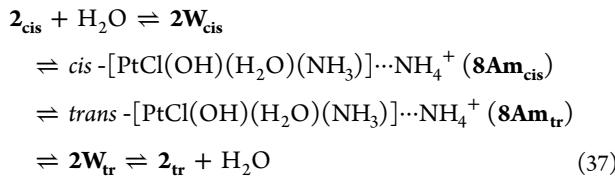


Figure 8. Geometries of transition states **TS_{2cis/2tr}** and **TS_{3cis/3tr}** in single-step reaction of cis-trans isomerization. Unit is angstroms.

exchange is not possible in eq 34. The intrinsic reaction coordinate (IRC) analysis supports that **TS_{2cis/2tr}** and **TS_{3cis/3tr}** directly connect the reactant and the product in eqs 35 and 36, respectively. The activation free energy in eq 35 was calculated to be 50.9 kcal/mol for the forward reaction and 49.2 kcal/mol for the backward reaction. Also, the activation free energy in eq 36 was calculated to be 56.1 kcal/mol for the forward reaction and 50.6 kcal/mol for the backward reaction. These very large activation free energies indicate that the cis-trans isomerization reactions in eqs 35 and 36 do not occur via single-step reaction through either **TS_{2cis/2tr}** or **TS_{3cis/3tr}**.

As an alternative path of multistep reactions in eqs 35 and 36, we found that the cis–trans isomerization reaction could occur in a stepwise manner through the substitution of the NH₃ ligand for the water molecule, as shown in eqs 37 and 38; see the Supporting Information, Figures S14 and S15, for details:



Figures S14 and S15 in the Supporting Information show the cis–trans isomerization between $\mathbf{2}_{\text{cis}}$ and $\mathbf{2}_{\text{tr}}$ and that between $\mathbf{3}_{\text{cis}}$ and $\mathbf{3}_{\text{tr}}$, respectively. In the cis–trans isomerization reaction between $\mathbf{2}_{\text{cis}}$ and $\mathbf{2}_{\text{tr}}$, the substitution of the NH₃ ligand for the water molecule occurs with the activation free energy of about 31 kcal/mol through a trigonal bipyramidal transition state $\mathbf{TS2d}$ (path 2D); this is similar to path 1A (or path 1B) in eq 30. In the same manner as the stepwise reactions of paths 1A and 1C and those of paths 1B and 1C (Figure 7), the substituted NH₃ ligand, which stays favorably in the first solvation shell ($\mathbf{8Am}_{\text{cis}}$), needs to migrate to the other H₂O ligand ($\mathbf{8Am}_{\text{tr}}$) and the substitution of the H₂O ligand for NH₃ must occur through transition state $\mathbf{TS2f}$ (path 2F); see Figure S14 in the Supporting Information. However, these reactions are more difficult than the stepwise reactions of paths 1A and 1C and those of paths 1B and 1C (Figure 7); $\mathbf{TS2d}$ and $\mathbf{TS2f}$ were about 10 kcal/mol higher in free energy than $\mathbf{TS1a}$ (or $\mathbf{TS1b}$) and $\mathbf{TS1c}$, respectively. This means that the cis–trans isomerization reaction does not occur via paths 2D and 2F; see Figure S14 in the Supporting Information. Also, as shown in Figure S15 in the Supporting Information, the cis–trans isomerization reaction between $\mathbf{3}_{\text{cis}}$ and $\mathbf{3}_{\text{tr}}$ is not easy because of the much higher free energies of $\mathbf{TS3d}$ and $\mathbf{TS3f}$; they are 55.1 and 55.7 kcal/mol.

5. CONCLUSION

To evaluate the ESP around the solute, which is necessary to solve the RISM integral equation, we newly introduced the switching function to smoothly connect the ESP directly calculated with the solute electronic wave function and that approximately calculated with the solute point charges. Introducing the switching function, we improved not only the energy calculation but also the analytical gradient calculation in the 3D-RISM-SCF method, where the solvent grid space was divided into the inner, outer, and switching regions. The direct calculation of the ESP in the inner and switching regions is very powerful to solve the divergence problem of the solute ESP charges with modest computational demands, though this problem sometimes happens in the RISM-SCF method based on the pure point charge protocol.

To investigate if the free energy profiles and the microscopic solvation structures are reliably presented by this method, we applied the present 3D-RISM-SCF method to the hydrolysis processes of cis- and transplatin. Here, we calculated the free

energy profiles of the hydrolyses at the CCSD(T) level with the MP2 evaluation of the basis set extension effect. Though the translational entropy in the condensed phase and the vibrational entropy of low frequency modes would cause some errors as are well-known, the present results agree with the experimental values of the activation free energy barriers and the experimental tendencies of the equilibrium constants in the hydrolyses of cis- and transplatin. Though the second hydrolysis has been investigated in the absence of the Cl counteranion in the first solvation shell, the present 3D-RISM-SCF study indicates that the second hydrolysis occurs to afford diaqua Pt complex without dissociation of the Cl counteranion from the first solvation shell of monoqua [PtCl(H₂O)(NH₃)₂]⁺ complex. This feature is close to the results by the CPMD and the QM/MM-MD simulations.

One of the strong points of the 3D-RISM-SCF method is to present the 3D solvation structure around a large transition metal complex. The 3D solvation structure indicates that the increase of the H_w-interacting water solvents around the substituted Cl ligand is crucial to accelerate both the first hydrolysis and the second hydrolysis while keeping the Cl anion in the first solvation shell. The solvation effect on the hydrolysis is different between cis- and transplatin. The 3D-RISM-SCF method provides a clear explanation about the difference. Here we theoretically investigated the cis–trans isomerization of platin because it has not been investigated yet. However, the cis–trans isomerization does not occur via Berry's pseudorotation. One possibility of the cis–trans isomerization is found in the stepwise reaction pathway through either the formation of $\text{trans}-[\text{PtCl}_2(\text{OH})(\text{NH}_3)]^-$ ($\mathbf{4}_{\text{tr}}$) and NH₄⁺ or that of $\text{trans}-[\text{PtCl}_2(\text{H}_2\text{O})(\text{NH}_3)]$ ($\mathbf{5}_{\text{tr}}$) and NH₃; $\mathbf{1}_{\text{cis}} + \text{W} \rightarrow \mathbf{2Cl}_{\text{cis}} \rightarrow \mathbf{4}_{\text{tr}} + \text{Am}^+$ or $\mathbf{5}_{\text{tr}} + \text{Am} \rightarrow \mathbf{1}_{\text{tr}} + \text{W}$ for the cis → trans isomerization and $\mathbf{1}_{\text{tr}} + \text{W} \rightarrow \mathbf{4}_{\text{tr}} + \text{Am}^+$ or $\mathbf{5}_{\text{tr}} + \text{Am} \rightarrow \mathbf{2Cl}_{\text{cis}} \rightarrow \mathbf{1}_{\text{cis}} + \text{W}$ for the trans → cis isomerization. Though the possibility is not large because of considerably larger activation free energy than the usual second hydrolysis, this would occur at high temperature, indicating that the hydrolysis of cisplatin must be performed under mild conditions.

■ ASSOCIATED CONTENT

5 Supporting Information

Complete ref 45, details of present 3D-RISM procedure, and additional data of solvent radial distribution function in hydrolyses, geometrical changes, and free energy profiles of usual hydrolyses, substitution of NH₃ ligand for water solvent, and cis–trans isomerization reactions. This material is available free of charge via the Internet at <http://pubs.acs.org>.

■ AUTHOR INFORMATION

Corresponding Author

*E-mail: sakaki.shigeyoshi.47e@st.kyoto-u.ac.jp.

Notes

The authors declare no competing financial interest.

■ ACKNOWLEDGMENTS

This work was financially supported by a Grant-in-Aid for Specially Promoted Science and Technology (No. 22000009) and a Grand Challenge Project (IMS, Okazaki, Japan) from the Ministry of Education, Culture, Sports, Science and Technology.

■ REFERENCES

- (1) Tomasi, J.; Persico, M. *Chem. Rev. (Washington, D.C.)* **1994**, *94*, 2027–2094. Tomasi, J.; Mennucci, B.; Cammi, R. *Chem. Rev. (Washington, D.C.)* **2005**, *105*, 2999–3093.
- (2) Cammi, R.; Tomasi, J. *J. Chem. Phys.* **1994**, *100*, 7495–7502; **1995**, *101*, 3888–3897. Cossi, M.; Mennucci, B.; Cammi, R. *J. Comput. Chem.* **1996**, *17*, 57–73.
- (3) Cramer, C. J.; Truhlar, D. G. *Chem. Rev. (Washington, D.C.)* **1999**, *99*, 2161–2200.
- (4) Chandler, D.; Anderson, H. C. *J. Chem. Phys.* **1972**, *57*, 1930–1931.
- (5) Hirata, F.; Rossky, P. J. *Chem. Phys. Lett.* **1981**, *83*, 329–334.
- (6) Ten-no, S.; Hirata, F.; Kato, S. *Chem. Phys. Lett.* **1993**, *214*, 391–396; *J. Chem. Phys.* **1994**, *100*, 7443–7453.
- (7) Sato, H.; Hirata, F.; Kato, S. *J. Chem. Phys.* **1996**, *105*, 1546–1551.
- (8) In the glucoside degradation, especially at the intramolecular O–H–O bridged bond in the sugar ring, the 1D-RISM-SCF method fails to determine the surrounding solvation structure.
- (9) Yokogawa, D.; Sato, H.; Sakaki, S. *J. Chem. Phys.* **2007**, *126*, 244504; *J. Chem. Phys.* **2009**, *131*, 214504.
- (10) Sato, H.; Kovalenko, A.; Hirata, F. *J. Chem. Phys.* **2000**, *112*, 9463–9468.
- (11) Yoshida, N.; Hirata, F. *J. Comput. Chem.* **2006**, *27*, 453–462.
- (12) Strictly speaking, the region near the solute includes the repulsive core region, where we do not have to evaluate the ESP because of a too large repulsive Lennard-Jones interaction, as proposed by the original method.¹¹ Though not explicitly represented here, the repulsive core region is implicitly involved in the inner region and practically treated.
- (13) The original method can easily define the arbitrary shape for the inner region and reduce the largest number of grids at the cost of continuity of solvent distribution.
- (14) Kaim, W.; Schwederski, B. *Bioinorganic Chemistry: Inorganic Elements in the Chemistry of Life*; John Wiley & Sons: Chichester, U.K., 1994; pp 367–371.
- (15) Rotzinger, F. P. *Chem. Rev.* **2005**, *105*, 2003–2037.
- (16) Sherman, S. E.; Gibson, D.; Wang, A. H. J.; Lippard, S. *J. J. Am. Chem. Soc.* **1988**, *110*, 7368–7381.
- (17) Arpalähti, J.; Mikola, M.; Mauristo, S. *Inorg. Chem.* **1993**, *32*, 3327–3332.
- (18) Mikola, M.; Arpalähti, J. *Inorg. Chem.* **1994**, *33*, 4439–4445.
- (19) Vinje, J.; Sletten, E.; Kozelka, J. *Chem.—Eur. J.* **2005**, *11*, 3863–3871.
- (20) Davies, M. S.; Berners-Price, S. J.; Hambley, T. W. *Inorg. Chem.* **2000**, *39*, 5603–5613.
- (21) Zhang, Y.; Guo, Z.; You, X.-Z. *J. Am. Chem. Soc.* **2001**, *123*, 9378–9387.
- (22) Burda, J. V.; Zeizinger, M.; Leszczynski, J. *J. Chem. Phys.* **2004**, *120*, 1253–1262.
- (23) Lau, J. K.-C.; Deubel, D. V. *J. Chem. Theory Comput.* **2006**, *2*, 103–106.
- (24) Melchior, A.; Marcos, E. S.; Pappalardo, R. R.; Martinez, J. M. *Theor. Chem. Acc.* **2011**, *128*, 627–638.
- (25) Cooper, J.; Ziegler, T. *Inorg. Chem.* **2002**, *41*, 6614–6622.
- (26) Baik, M.-H.; Friesner, R. A.; Lippard, S. *J. J. Am. Chem. Soc.* **2003**, *125*, 14082–14092.
- (27) Costa, L. A. S.; Rocha, W. R.; De Almeida, W. B.; Dos Santos, H. F. *J. Chem. Phys.* **2003**, *118*, 10584–10592.
- (28) Zimmerman, T.; Chval, Z.; Burda, J. V. *J. Phys. Chem. B* **2009**, *113*, 3139–3150.
- (29) Lopes, J. F.; de A. Menezes, V. S.; Duarte, H. A.; Rocha, W. R.; De Almeida, W. B.; Dos Santos, H. F. *J. Phys. Chem. B* **2006**, *110*, 12047–12054.
- (30) Carloni, P.; Sprik, M.; Andreoni, W. *J. Phys. Chem. B* **2000**, *104*, 823–835.
- (31) Lau, J. K.-C.; Ensing, B. *Phys. Chem. Chem. Phys.* **2010**, *12*, 10348–10355.
- (32) Beret, E. C.; Martinez, J. M.; Pappalardo, R. R.; Marcos, E. S.; Dotsis, N. L.; Marx, D. *J. Chem. Theory Comput.* **2008**, *4*, 2108–2121.
- (33) Yokogawa, D.; Ono, K.; Sato, H.; Sakaki, S. *Dalton Trans.* **2011**, *40*, 11125–11130.
- (34) *The Merck Index*, 12th ed.; entry no. 2378.
- (35) Breusova-Baidala, Y. G.; Zheligovskaya, N. N.; Spitsyn, V. I. *Izv. Akad. Nauk SSSR, Ser. Khim.* **1974**, *6*, 1239–1242.
- (36) Dupuis, M.; Rys, J.; King, H. F. *J. Chem. Phys.* **1976**, *65*, 111–116.
- (37) In the standard QM calculation in the gas phase, $A_{\mu\nu}(\mathbf{r})$ terms must be evaluated only at the atomic sites, indicating that the evaluation of two-electron integrals is much more time-consuming than that of one-electron integrals. However, in the 3D-RISM-SCF calculation with the explicit evaluation of the ESP, the evaluation of $A_{\mu\nu}(\mathbf{r})$ at all points of the solvent grid space ($O(N^3)$) needs significantly long CPU time, because N (points/axis of solvent grid space) is usually taken to be greater than 128. Our improvement with the switching function significantly reduces the CPU time; see the Supporting Information, Table S2, for details.
- (38) Boys, S. F.; Bernardi, F. B. *Mol. Phys.* **1970**, *19*, 553–566.
- (39) Mori, T.; Kato, S. *Chem. Phys. Lett.* **2007**, *437*, 159–163.
- (40) Cammi, R.; Olivares Del Valle, F. J.; Tomasi, J. *Chem. Phys.* **1988**, *122*, 63–74.
- (41) Mammen, M.; Shakhnovich, E. I.; Deutch, J. M.; Whitesides, G. M. *J. Org. Chem.* **1998**, *63*, 3821–3830.
- (42) Berendsen, H. J. C.; Postma, J. P. M.; van Gunstern, W. F.; Hermans, J. *Intermolecular Forces*; Pullman, B., Ed.; Reidel: Dordrecht, The Netherlands, 1981; pp 331–342.
- (43) Cornell, W. D.; Cieplak, P.; Bayly, C. I.; Gould, I. R.; Merz, K. M., Jr.; Ferguson, D. M.; Spellmeyer, D. C.; Fox, T.; Caldwell, J. W.; Kollman, P. A. *J. Am. Chem. Soc.* **1995**, *117*, 5179–5197.
- (44) Hayaki, S.; Yokogawa, D.; Sato, H.; Sakaki, S. *Chem. Phys. Lett.* **2008**, *458*, 329–332.
- (45) Schmidt, M. W.; et al. *J. Comput. Chem.* **1993**, *14*, 1347–1363 (See the Supporting Information for the complete reference.).
- (46) Milburn, G. H. W.; Truter, M. R. *J. Chem. Soc. A* **1966**, 1609–1616.
- (47) Some of these important geometries were not successfully optimized by the usual 1D- and 3D-RISM-SCF calculations with the pure point charge approximation because of the diverged ESP charges of the solute.
- (48) The present 3D-RISM-SCF analysis is based on the solvent model with the nonpolarizable force field. If the solvent polarization effect is taken into consideration, the solute–solvent interaction becomes stronger and hence the solvation free energy becomes larger. This means that the calculated activation free energy and reaction free energy in this reaction are moderately overestimated in the present RISM-SCF study, because the product and the transition state are more stabilized by solvation than the reactant.
- (49) Though the surrounding solvents are treated implicitly as the probability density functions in the RISM-SCF method, a lot of water solvent molecules always exist near the Pt complex of **1**+**W** (or **2**+**W**) as the candidate of the substrate water in the hydrolysis. In the present calculation, we evaluated the activation free energy of the first hydrolysis by the free energy difference between **1****W** and **TS1** and that of the second hydrolysis by the free energy difference between **2****W** and **TS2**, because the numerical error coming from the translational entropy can be omitted.
- (50) Perumareddi, J. R.; Adamson, A. W. *J. Phys. Chem.* **1978**, *72*, 414–420.
- (51) Hindmarsh, K.; House, D. A.; Turnbull, M. M. *Inorg. Chim. Acta* **1997**, *257*, 11–18.
- (52) Glendening, E. D.; Badenhoop, J. K.; Reed, A. E.; Carpenter, J. E.; Bohmann, J. A.; Morales, C. M.; Weinhold, F. *NBO 5.0*; Theoretical Chemistry Institute, University of Wisconsin: Madison, 2001.
- (53) In transplatin, the Cl–Pt–Cl angle (180°) in **RAS1_{tr}** decreases to 143° in **TS1_{tr}** and then to 126° in **2Cl_{tr}**. This decrease of the Cl–

Pt–Cl angle also supports the tendency that the dipole moment of transplatin species monotonically increases from **1W_{tr}** to **2Cl_{tr}**, as shown in Table 2.

(54) Kubo, R.; Toda, M.; Hashitsume, N. *Statistical Physics II: Nonequilibrium Statistical Mechanics*, 2nd ed.; Springer-Verlag: Berlin, 1991; pp 146–202.

(55) Levy, R. M.; Belhadj, M.; Kitchen, D. B. *J. Chem. Phys.* **1991**, *95*, 3627–3633.

(56) Vener, M. V.; Leontyev, I. V.; Dyakov, Y. A.; Basilevsky, M. V.; Newton, M. D. *J. Phys. Chem. B* **2002**, *106*, 13078–13088.

(57) Yamazaki, S.; Kato, S. *J. Chem. Phys.* **2005**, *123*, 114510.

(58) Mori, T.; Kato, S. *J. Chem. Phys.* **2010**, *133*, 064107.

(59) Aono, S.; Minezawa, N.; Kato, S. *Chem. Phys. Lett.* **2010**, *492*, 193–197.

(60) Aono, S.; Yamamoto, T.; Kato, S. *J. Chem. Phys.* **2011**, *134*, 144108.

(61) Considering that the free energy does not increase very much by the Cl dissociation, we cannot rule out the second hydrolysis with Cl dissociation.

(62) Berry, R. S. *J. Chem. Phys.* **1960**, *32*, 933–938.